

Rule-Based Lloyd Algorithm for Multi-Robot Motion Planning and Control with Safety and Convergence Guarantees

Manuel Boldrer, Álvaro Serra-Gómez, Lorenzo Lyons, Vít Krátký, Javier Alonso-Mora, Laura Ferranti

Abstract—This paper presents a distributed rule-based Lloyd algorithm (RBL) for multi-robot motion planning and control. The main limitations of the basic Lloyd-based algorithm (LB) concern deadlock issues and the failure to address dynamic constraints effectively. Our contribution is twofold. First, we show how RBL is able to provide safety and convergence to the goal region without relying on communication between robots, nor synchronization between the robots. We considered different dynamic constraints with control inputs saturation. Second, we show that the Lloyd-based algorithm (without rules) can be successfully used as a safety layer for learning-based approaches, leading to non-negligible benefits. We further prove the soundness, reliability, and scalability of RBL through extensive simulations, comparisons with the state of the art, and experimental validations on small-scale car-like robots, unicycle-like robots, omnidirectional robots, and aerial robots on the field.

Index Terms—Multi-Robot Systems, Distributed Control, Lloyd-based algorithms.

I. INTRODUCTION

The rise of mobile robotics is poised to have a significant impact on our daily lives in the near future. One essential skill that autonomous robots must have is the ability to move from one location to another. However, this task can be quite challenging, particularly in environments shared with other robots. An effective motion planning and control algorithm should prioritize three key aspects: safety, security, and convergence towards the intended destination.

Safety is of utmost importance, each robot should be equipped with collision avoidance capabilities to prevent accidents with other robots or assets. Additionally, security measures, such as reducing (or completely removing) reliance on the communication network or employing algorithms that are resilient against attacks and packet losses/delays, should be implemented to ensure the robustness of the system. Finally, successful convergence towards the intended destination requires avoiding the occurrence of deadlocks and live-locks, where deadlocks refer to situations where robots are stuck and unable to proceed due to conflicting actions, while live-locks involve continuous repetitive actions that prevent progress

towards the desired goal location. In this work we address all the aforementioned issues by employing a novel Rule-Based Lloyd solution.

A. Related works

Multi-robot motion planning and control can be broadly categorized into two main approaches: *centralized* and *distributed* methods. Centralized approaches in multi-robot motion planning and control involve a central unit responsible for computing control inputs for all the robots in the system. These methods offer the advantage of achieving optimal solutions more easily. However, they face scalability issues when the number of robots increases, and they have to rely on a dependable communication network to exchange real-time information between the coordinator and the robots. Centralized approaches can be particularly valuable in well-structured environments such as warehouses [1], [2], where optimizing the solution is of utmost importance.

In contrast, distributed approaches in multi-robot motion planning and control involve individual robots computing their own control inputs using local information. While these methods may yield sub-optimal solutions, they offer advantages in terms of scalability and robustness compared to centralized approaches. Distributed methods are capable of handling a larger number of robots and are more resilient to communication failures or limitations. They allow robots to make decisions based on local perception, which can be beneficial in dynamic and uncertain environments.

After opting to explore distributed methods due to their significant advantages over centralized approaches, we can identify three primary categories for multi-robot motion planning and control [3]: *reactive*, *predictive planning*, *learned-based* methods.

1) *Reactive methods*: are myopic by definition, hence each action is taken on the basis of the current local state. Despite being computationally efficient and usually easy to implement, deadlock conditions (local minima) as well as live-lock may occur, preventing the robots to reach the goal positions. The most popular approaches rely on velocity obstacles [4]–[11], force fields [12]–[14], barrier certificates [15]–[17], and dynamic window [18].

2) *Predictive planning methods*: use information about the neighboring robots in order to plan optimal solutions. Even though they can substantially increase the performance metrics and may avoid deadlocks by increasing the prediction horizon,

M. Boldrer and V. Krátký are with the Dept. of Cybernetics, Czech Technical University, Karlovo namesti 13, 12135, Prague, Czechia, {boldrman, kratkvit}@fel.cvut.cz. A. Serra-Gómez, L. Lyons, J. Alonso-Mora, L. Ferranti are with the Dept. of Cognitive Robotics, Delft University of Technology, Mekelweg 2, 2628 CD, Delft, Netherlands, {a.serragomez, l.lyons, j.alonsomora, l.ferranti}@tudelft.nl.

This research is supported by the NWO-TTW Veni project HARMONIA (no. 18165).

usually they can be computationally expensive and/or the robots need to exchange a large amount of information through the communication network, which may not be highly reliable. Moreover, these methods may fall in live-lock conditions, which prevent the robots to converge to the goal positions. Solutions based on assigning priorities (sequential solutions) or synchronous re-planning are adopted to avoid this problem, but in the former case it introduces a hierarchy among the agents, in the latter a global clock synchronization is required. The most popular approaches rely on model predictive control (MPC) [19]–[26], elastic bands [27], buffered Voronoi cells [28]–[31], legible motion [32], [33] and linear spatial separations [34]. Other interesting and recent solutions are provided by [35]–[43], all of them relying on a communication network.

3) *Learning-based methods*: are promising and many researchers are investigating their potential [44]–[58]. However, the weakness of these approaches is related to the lack of guarantees, especially for safety and convergence. In addition, the solution that these approaches provide are often non-explainable and generalization to situations different from the training scenario are hard to provide (e.g., number of robots, robots' encumbrance, robots' dynamics and velocities). With respect to the state of the art algorithms, our solution allows the robots to avoid collisions and converge to their goal regions without relying on communication, without relying on the neighbors' control inputs, and without the need of synchronization. In the literature, the main approaches that rely only on neighbors positions and encumbrances, and hence do not require communication between the robots, are BVC [28], RLSS [34] and SBC [15], but none of them achieves a success rate of 1.00 in very crowded scenarios. In fact, we tested BVC and SBC in environments with a crowdness factor $\eta = 0.452$; both of them result in a success rate $SR = 0.00$. On the other hand, RLSS has a higher success rate; however, it can experience deadlock/live-lock issues, as well as safety issues in an asynchronous setting (see [39]). This is a severe problem also due to their required computational time, which in average is greater than 100 (ms).

Our algorithm prove to be a valid solution in scenarios where communication between robots is unfeasible. This situation can arise from several reasons, such as security concerns, cost reduction initiatives, the necessity for interactions between diverse robots from different companies, adversarial environmental conditions, or simply for technological limitations [59]. A safe and networkless motion planning and control algorithm can find plenty of applications including but not limited to agriculture-related applications, environmental monitoring, delivery services, warehouse and logistics, space exploration, search and rescue among others.

B. Paper contribution and organization

This paper proposes a distributed algorithm for multi-robot motion planning and control. Our contribution is twofold.

Firstly, we synthesize what we called the rule-based Lloyd algorithm (RBL), a solution that can guarantee safety and convergence towards the goal region. With respect to our previous

work [60], here we focused on the interaction between robots and: 1) We drastically improve the multi-robot coordination performance, that is, we increased the success rate from 0.00 to 1.00 in scenarios with more than 20 robots; 2) We provide, not only safety, but also sufficient conditions for convergence towards the goal regions; and 3) We extend the algorithm to account for dynamic constraints and control inputs saturation by leveraging on model predictive controller (MPC). Secondly, we show how the basic Lloyd-based algorithm (without rules) can be used effectively as a *safety layer* in learning-based methods. We present the Learning Lloyd-based algorithm (LLB), where we used reinforcement learning [61] to synthesize a motion policy that is intrinsically safe both during learning and during testing. We show that it benefits the learning phase, enhancing performance, since safety issues are already solved. By using the Lloyd-based support, in comparison to the same learning approach without the support (pure learning), we measure an increase of the success rate from 0.56 to 1.00 in simple scenarios with 5 robots, until an increase from 0.00 to 1.00 in more challenging scenarios with 50 robots. Notice that, while RBL has guarantees with respect to the convergence to the goal, on the other hand, LLB does not ensure convergence. Nevertheless, it may perform better in terms of travel time in certain scenarios.

The paper is organized as follows. Sec. II provides the problem description. Sec. III describes the proposed algorithms. Sec. IV provides simulation results and an updated comparison with the state of the art. Sec. V provides experimental results. Finally, Sec. VI concludes the paper.

II. PROBLEM DESCRIPTION

Our goal is to solve the following problem:

Problem 1. Given N robots, we want to steer each of them from the initial position $p_i(0)$ towards a goal region defined as the ball set $\mathcal{B}(e_i, \varepsilon)$ centered in e_i , with radius ε . We want to do it reliably in a safe and communication-less fashion.

Assumption 1. Each robot knows its position p_i , its encumbrance δ_i , which defines the radius of the circle enclosing the robot, as well as the positions and encumbrances of its neighboring robots, i.e., $j \in \mathcal{N}_i$ if $\|p_i - p_j\| \leq 2r_{s,i}$, where \mathcal{N}_i denotes the set comprising the neighbors of the i -th robot, while $r_{s,i} = r_s$ is assumed to be the same for all the robots and it is defined as half of the sensing radius. In practice, both localization and neighbor detection, can be done by means of a localization module (e.g., GPS, encoders, cameras, IMU) and a vision module (e.g., cameras, Lidar).

Assumption 2. To provide convergence guarantees, we assume that the mission space is an unbounded convex space. Notice that the algorithm would preserve safety even in cluttered environments [62], however it would entail making extra assumptions to prove the convergence.

III. APPROACH

The proposed approach is based on the Lloyd algorithm [63]. The main idea is to consider the following cost

function

$$J_{\text{cov}}(p) = \sum_{i=1}^n \int_{\mathcal{V}_i} \|q - p_i\|^2 \varphi_i(q) dq, \quad (1)$$

which was originally used in [64] for static coverage control, where the positions of the robots are represented by $p = [p_1, \dots, p_N]^\top$, $p_i = [x_i, y_i]^\top$, the mission space is denoted by \mathcal{Q} , the weighting function that measures the importance of the points $q \in \mathcal{Q}$ is denoted by $\varphi_i(q) : \mathcal{Q} \rightarrow \mathbb{R}_+$ and \mathcal{V}_i indicates the Voronoi cell for the i -th robot, which is defined as

$$\mathcal{V}_i(p) = \{q \in \mathcal{Q} \mid \|q - p_i\| \leq \|q - p_j\|, \forall j \neq i\}. \quad (2)$$

Under the assumption of single integrator dynamics $\dot{p}_i = u_i$, and by following the gradient descent $\nabla J_{\text{cov}} = \frac{\partial J_{\text{cov}}(p)}{\partial p_i}$, it follows the proportional control law

$$\dot{p}_i(\mathcal{V}_i) = -k_{p,i}(p_i - c_{\mathcal{V}_i}), \quad (3)$$

where the tuning parameter $k_{p,i} > 0$ is a positive value, and

$$c_{\mathcal{V}_i} = \frac{\int_{\mathcal{V}_i} q \varphi_i(q) dq}{\int_{\mathcal{V}_i} \varphi_i(q) dq} \quad (4)$$

is defined as the centroid position computed over the i -th Voronoi cell. It can be proved that by imposing (3) and assuming a time-invariant $\varphi_i(q)$, each robot converges asymptotically to its Voronoi centroid position. Our claim is that, by modifying the geometry of the cell \mathcal{V}_i and by properly designing a weighting function $\varphi_i(q)$, we can obtain an efficient and effective algorithm for multi-robot motion planning and control. Notice that, while the cell geometry to provide safety was introduced by the basic LB algorithm [60], [62], [65]–[67], one of the novelty introduced in this work, besides the use of the algorithm as a safety layer for learning-based algorithm and the introduction of an MPC formulation to deal with dynamical constraints, is the addition of rules in the shaping of the weighting function $\varphi_i(q)$, which are crucial in order to increase the performance and provide convergence guarantees to the goal positions.

A. Cell geometry \mathcal{A}_i

The reshape of the cell geometry is necessary and sufficient to provide safety guarantees. By relying on the classical Voronoi partition (2), we do not account for the encumbrances of the robots in the scene, and neither for the limited sensing range of the robots' sensors. Hence, as was proposed in our previous works [60], [67], we defined the cell $\mathcal{A}_i = \{\tilde{\mathcal{V}}_i \cap \mathcal{S}_i\}$, where

$$\tilde{\mathcal{V}}_i = \begin{cases} \{q \in \mathcal{Q} \mid \|q - p_i\| \leq \|q - p_j\|\} & \text{if } \Delta_{ij} \leq \frac{\|p_i - p_j\|}{2} \\ \{q \in \mathcal{Q} \mid \|q - p_i\| \leq \|q - \tilde{p}_j\|\} & \text{otherwise,} \end{cases} \quad (5)$$

$\forall j \in \mathcal{N}_i$, where $\Delta_{ij} = \delta_j + \delta_i$ is the sum of the radius of encumbrance of robots i and j , and $\tilde{p}_j = p_j + 2\left(\Delta_{ij} - \frac{\|p_i - p_j\|}{2}\right) \frac{p_i - p_j}{\|p_i - p_j\|}$, takes into account the encumbrance of the robots, while

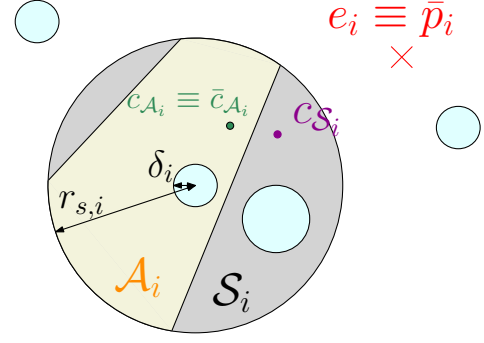


Figure 1: We depicted the robots as blue circles and the main parameters and variables associated with robot i .

$$\mathcal{S}_i = \{q \in \mathcal{Q} \mid \|q - p_i\| \leq r_{s,i}\}. \quad (6)$$

Theorem 1 (Safety). *By imposing the control $\dot{p}_i(\mathcal{A}_i)$ in (3), collision avoidance is guaranteed at every instant of time.*

Proof. Since the set $\mathcal{A}_i = \{\tilde{\mathcal{V}}_i \cap \mathcal{S}_i\}$ is a convex set, then the centroid position $c_{\mathcal{A}_i} \in \mathcal{A}_i$. By definition of convex set, there exists a straight path from p_i towards the centroid $c_{\mathcal{A}_i}$. Since $p_i, c_{\mathcal{A}_i} \in \{\tilde{\mathcal{V}}_i \cap \mathcal{S}_i\}$, by exploiting the definition of convex set, we ensure that the path towards the centroid is a safe path (i.e., no other robots on the path towards the centroid), hence the control law $\dot{p}_i(\mathcal{A}_i)$ as (3) always preserves safety. \square

B. The weighting function $\varphi_i(q)$

While the safety can be guaranteed by properly shaping the cell geometry, the convergence and the performance mainly depend on the definition of the function $\varphi_i(q)$. We adopt a Laplacian distribution centered at \bar{p}_i , which represents a point in the mission space that ultimately needs to converge to the goal location. Then we define the function $\varphi_i(q)$ as follows:

$$\varphi_i(q) = \exp\left(-\frac{\|q - \bar{p}_i\|}{\beta_i}\right) \quad (7)$$

where

$$\dot{\beta}_i(\mathcal{A}_i) = \begin{cases} -\beta_i & \text{if } \|c_{\mathcal{A}_i} - p_i\| < d_1 \wedge \\ & \|c_{\mathcal{A}_i} - c_{\mathcal{S}_i}\| > d_2 \\ -(\beta_i - \beta_i^D) & \text{otherwise.} \end{cases} \quad (8)$$

$$\dot{\bar{p}}_i = \begin{cases} -(\bar{p}_i - R^{p_i}(\pi/2 - \epsilon)e_i) & \text{if } \|c_{\mathcal{A}_i} - p_i\| < d_3 \wedge \\ & \|c_{\mathcal{A}_i} - c_{\mathcal{S}_i}\| > d_4 \\ -(\bar{p}_i - e_i) & \text{otherwise,} \end{cases}$$

$$\bar{p}_i = e_i \text{ if } \|p_i - \bar{c}_{\mathcal{A}_i}\| > \|p_i - c_{\mathcal{A}_i}\| \wedge \bar{p}_i = R^{p_i}(\pi/2 - \epsilon)e_i. \quad (9)$$

Notice that $\beta_i^D, d_1, d_2, d_3, d_4$ are positive scalar values, $R^{p_i}(\theta)$ indicates the rotation matrix centered in p_i , ϵ is a small number, e_i is the i -th robot final goal position, while $\bar{c}_{\mathcal{A}_i}$ is the centroid position computed over the cell \mathcal{A}_i with $\bar{p}_i \equiv e_i$.

For the sake of clarity in Figure 1 we depicted the main variables and parameters for the i -th robot.

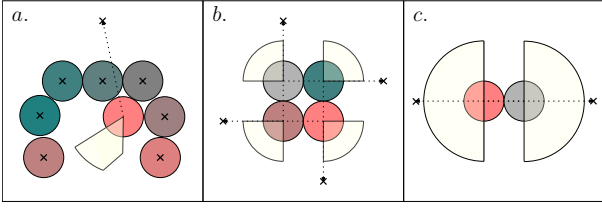


Figure 2: Theoretical deadlocking configurations, where $\beta_i = 0$, $\forall i = 1 \dots N$. The crosses indicates the final goal positions for the robots (blue circles). The set \mathcal{A}_i is depicted in yellow.

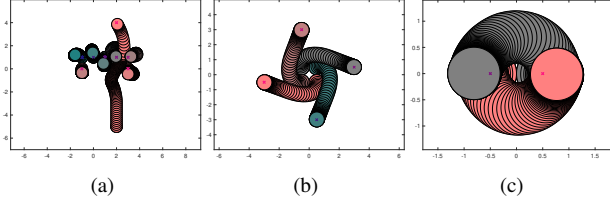


Figure 3: Simulation results starting from the theoretical deadlock conditions in Figure 2. The desired spreading factor is selected as $\beta^D = 0.5$ for every robot.

Proposition 1 (Convergence). Let us assume to have an unbounded convex space and that the initial and goal positions are adequately apart from each other, i.e., $\|p_i(0) - p_j(0)\| > \Delta_{ij}$, $\|e_i - e_j\| > \Delta_{ij}$, $\forall i, j = 1 \dots N$ with $i \neq j$.

By imposing the control law $\dot{p}_i(\mathcal{A}_i)$ in (3) and (7), (8), (9) to compute the centroid position in (4), and by selecting $d_1 = d_3$, $d_2 = d_4$ where $d_1 + d_2 > \|p_i - c_{S_i}\|$, $d_1 < \|p_i - c_{S_i}\|$ and $d_2 < \|p_i - c_{S_i}\|$, with $\beta_i^D > 0$, we have that $\lim_{t \rightarrow \infty} \|p_i(t) - e_i\| < r_{s,i}$, $\forall i = 1, \dots, N$.

Proof. The proof is structured as follows: first we ensure deadlock avoidance, then we guarantee live-lock avoidance and finally convergence. The i -th robot is in a deadlock condition, if it exists a time t_0 such that $\forall t \geq t_0$, $p_i(t_0) = p_i(t)$ and $p_i(t) \notin \mathcal{B}(e_i, r_{s,i})$. This condition is verified when $p_i \equiv c_{\mathcal{A}_i} \equiv \bar{c}_{\mathcal{A}_i}$ and $p_i \notin \mathcal{B}(e_i, r_{s,i})$, $\forall t \geq t_0$. In plain words, when the robot is outside of its goal region and its control inputs are zero for the rest of the mission. By accounting for the effects of (8), if a robot is in a deadlock condition it means that $\beta_i \rightarrow 0$ and at the same time the centroid position $c_{\mathcal{A}_i}$ does not move, thus deadlock can occur in two situations: *i.* if $p_i \equiv \bar{c}_{\mathcal{A}_i} \equiv c_{\mathcal{A}_i} \equiv \mathcal{A}_i$ and *ii.* if $p_i \equiv \bar{c}_{\mathcal{A}_i} \equiv c_{\mathcal{A}_i} \in \partial \mathcal{A}_i$, where $\partial \mathcal{A}_i$ indicates the contour of the \mathcal{A}_i set. Notice that *i.* \implies *ii.* but not the contrary. The case *i.* is a transitory condition if the external robots are not in condition *ii.*, hence we can only focus on the second condition. Notice that the existence of external robots is ensured by the fact that we assumed an infinite convex space.

For the condition *ii.* there exist three basic scenarios that satisfy the deadlocking conditions $p_i \equiv \bar{c}_{\mathcal{A}_i} \equiv c_{\mathcal{A}_i} \in \partial \mathcal{A}_i$, $\forall t \geq t_0$, with $p_i \notin \mathcal{B}(e_i, r_{s,i})$. More complex cases can be decomposed in one of the three scenarios or in a combination of them. We recognize that if the robots in the scene did not reach yet their goal locations the only chance of having a deadlock condition is to have a symmetric scenario, hence positions and goals of the robots have to be disposed

symmetrically. This is justified by the fact that asymmetric conditions lead the centroid positions away from p_i , denying deadlock condition. The remaining case is when only robot i did not reach its goal position, despite in general this is an asymmetrical scenario, if the robots physically hinder the i -th robot motion, deadlock conditions are met. We depict these scenarios in Fig. 2 for the sake of clarity, while in Fig. 3 we report the simulation results obtained by imposing the robots' initial conditions to be equal to the theoretical deadlock conditions of Fig. 2. In accordance with the simulation results, we claim that the deadlocks in cases *a.*, *b.*, and *c.* cannot occur by applying the rules (8) and (9). Notice that, the introduction of these rules is the main reason why RBL over performs LB [60] in success rate. Let us analyze the three scenarios:

Case a (Fig. 2-a): A certain number of robots have already reached their goal positions and they hinder the advancement of other robots that did not yet reach their goal locations. In this case, the value of d_2 in (8) has to be selected in such a way that β_i starts to decrease after an abundant deflection from the goal, e.g., $r_{s,i} > d_2 \geq 3\delta_{\max}$, where δ_{\max} is the encumbrance of the biggest robot in the mission space, notice that, by geometry, if $d_2 \geq 3\delta_{\max}$ it allows the passage of the robots in any scenario. In this way, by having that $\beta_i^D > 0$, each robot can be deflected from its goal position by a distance greater than d_2 .

This fact can be shown by computing the distance from the centroid position analytically. To simplify the notation, without loss of generality, we change reference frame, by considering $p_i = [0, 0]^T$ as our new origin. Hence we can write

$$\|p_i - c_{\mathcal{A}_i}\| = \left\| \frac{\int_0^{r_{s,i}} z \exp\left(-\frac{|z|}{\beta_i}\right) dz}{\int_0^{r_{s,i}} \exp\left(-\frac{|z|}{\beta_i}\right) dz} \right\|.$$

We considered the case where we have the i -th robot in its goal position e_i , and a neighbor robot j at distance $\Delta_{ij} = \delta_i + \delta_j$. By solving the integral we obtain

$$\|p_i - c_{\mathcal{A}_i}\| = \left\| \frac{(r_{s,i} + \beta_i) \exp\left(-\frac{r_{s,i}}{\beta_i}\right) - \beta_i}{\exp\left(-\frac{r_{s,i}}{\beta_i}\right) - 1} \right\|$$

hence, as the value of β_i increases, the distance $\|p_i - c_{\mathcal{A}_i}\|$ increases as well, moreover even when the robot moves from its goal, if the value of β_i does not change and the robot j continues to push towards robot i , then the distance $\|p_i - c_{\mathcal{A}_i}\|$ does not change:

$$\begin{aligned} \|p_i - c_{\mathcal{A}_i}\| &= \left\| \frac{\int_{-r_{s,i}}^0 z \exp\left(-\frac{|z-Kr_{s,i}|}{\beta_i}\right) dz}{\int_{-r_{s,i}}^0 \exp\left(-\frac{|z-Kr_{s,i}|}{\beta_i}\right) dz} \right\| \\ &= \left\| \frac{-\beta_i \exp\left(\frac{r_{s,i}}{\beta_i}\right) + r_{s,i} + \beta_i}{\exp\left(\frac{r_{s,i}}{\beta_i}\right) - 1} \right\|. \end{aligned} \quad (10)$$

In fact, $K > 0$ is an arbitrary value that quantifies the distance of e_i and it does not affect the centroid position according to (10), hence the i -th robot can be pushed away from its goal position by the robot j at least of a quantity equal to d_2 .

Case b (Fig. 2-b): It is an unstable and unreachable equilibrium, since a small perturbation will lead to leave this configuration and moreover, it is an equilibrium only if $\beta_i = 0$ for each robot, i.e., the centroids have to be positioned on the vertex of the cells; this is not possible since $\beta_i^D > 0$ and β_i evolves as (8).

Case c (Fig. 2-c): Due to the perfect symmetry, this case would be a deadlock condition if (9) does not activate (the parameters d_3, d_4 have to be chosen properly). Because of the directional asymmetry introduced by the right hand side behavior the robots do not fall in deadlock. The same consideration can be done in similar conditions with $N > 2$.

Notice that the values d_1, d_2, d_3, d_4 should depend on $r_{s,i}$, β^D and δ_{\max} , i.e., it is necessary that the conditions $\|c_{\mathcal{A}_i} - c_{\mathcal{S}_i}\| > d_2$ and $\|c_{\mathcal{A}_i} - c_{\mathcal{S}_i}\| > d_4$ can be verified, the conditions $\|c_{\mathcal{A}_i} - p_i\| < d_1$ and $\|c_{\mathcal{A}_i} - p_i\| < d_3$ do not have to be always verified, and $\|c_{\mathcal{A}_i} - c_{\mathcal{S}_i}\| > d_2 \implies \|c_{\mathcal{A}_i} - p_i\| < d_1$. By satisfying these requirements we have that the rules (7) and (8) during the mission can be engaged and disengaged. Let us assume to select $d_1 = d_3$ and $d_2 = d_4$. We can easily satisfy the requirements by imposing $d_1 + d_2 > \|p_i - c_{\mathcal{S}_i}\|$, $d_1 < \|p_i - c_{\mathcal{S}_i}\|$ and $d_2 < \|p_i - c_{\mathcal{S}_i}\|$. To compute the values d_1, d_2 and β^D on the basis of $r_{s,i}$, we can compute the following distance

$$\|p_i - c_{\mathcal{S}_i}\| = \left\| \frac{\int_{-r_{s,i}}^{r_{s,i}} z \exp\left(-\frac{|z - Kr_{s,i}|}{\beta_i}\right) dz}{\int_{-r_{s,i}}^{r_{s,i}} \exp\left(-\frac{|z - Kr_{s,i}|}{\beta_i}\right) dz} \right\|. \quad (11)$$

By considering $K \geq 1$ (i.e., $\|p_i - e_i\| > r_{s,i}$), $\beta_i = \beta_i^D$ and $r_{s,i} > 0$, we obtain

$$\|p_i - c_{\mathcal{S}_i}\| = \left\| \frac{(r_{s,i} - \beta_i^D) \exp\left(\frac{2r_{s,i}}{\beta_i^D}\right) + r_{s,i} + \beta_i^D}{\exp\left(\frac{2r_{s,i}}{\beta_i^D}\right) - 1} \right\| \quad (12)$$

hence by selecting $d_1 + d_2 > \|p_i - c_{\mathcal{S}_i}\|$, $d_1 < \|p_i - c_{\mathcal{S}_i}\|$ and $d_2 < \|p_i - c_{\mathcal{S}_i}\|$, where $\|p_i - c_{\mathcal{S}_i}\|$ is defined as in (12), then, by geometry, our requirements are satisfied. In Remark 1 we provide an example for a proper selection of the parameters.

Once we verified deadlock avoidance, we have to check for live-lock avoidance. The i -th robot is in a live-lock condition if it exists a time t_0 , such that $\forall t > t_0$, the control input sequence $\{u_i(t_k)\}_{k=0}^n$ is repeated and $p_i(t) \notin \mathcal{B}(e_i, r_{s,i})$. This kind of cyclic motions can be induced either by (8) or by (9). Notice that, if the functions $\varphi_i(q)$ are time-invariant, cyclic motions are not possible, since the robots converge to their centroids positions [64]. In fact, by considering $J_{\text{cov}}(p, \mathcal{A})$ (1) as a Lyapunov function:

$$\begin{aligned} \frac{d}{dt} J_{\text{cov}}(p, \mathcal{A}) &= \sum_{i=1}^n \frac{\partial}{\partial p_i} J_{\text{cov}}(p, \mathcal{A}) \dot{p}_i \\ &= \sum_{i=1}^n 2m_i (p_i - c_{\mathcal{A}_i})^T (-k_{p,i} (p_i - c_{\mathcal{A}_i})) \\ &= -2k_{p,i} \sum_{i=1}^n m_i \|p_i - c_{\mathcal{A}_i}\|^2, \end{aligned}$$

where $m_i = \int_{\mathcal{A}_i} \varphi_i(q) dq$, we have convergence towards the centroid by the LaSalle's invariance principle.

A cyclic back and forth motion can be introduced by (8), however, by construction it can happen only in the proximity of the goal and if the goal positions of two or more robots are close one each others.

On the other hand, a cyclic motion can be introduced by (9) as well. In this case, since we do not have deadlock conditions, by construction it may occur only if two or more robots have a close goal position, that is, $\|e_i - e_j\| < \Delta_{ij}$, which violates our assumption. In fact the other possible case would be when the robot is constantly hindered by other robots to reach its goal position. However, this is not possible since deadlock does not occur and because each robot can be deflected from its goal (see *case a*). Notice that the role of the reset condition $\bar{p}_i = e_i$ in (9) plays a crucial role since slow dynamics may lead to periodic motions.

Since all the robots converge asymptotically to their own centroid $c_{\mathcal{A}_i}$ by the LaSalle's principle, and deadlock/live-lock (if $\|p_i - e_i\| > r_{s,i}$) do not occur, then all the robots will converge to their centroids' positions (or, if live-lock occurs, inside $\mathcal{B}(e_i, r_{s,i})$), which satisfy $\|c_{\mathcal{A}_i} - e_i\| < r_{s,i}$, hence the proof is complete. \square

Remark 1 (Parameter Selection). Notice that to obtain convergence, a possible selection of the parameters in (8), (9) is the following. As we state in the proof of Proposition 1, provided that

$$\left\| \frac{(r_{s,i} - \beta_i^D) \exp\left(\frac{2r_{s,i}}{\beta_i^D}\right) + r_{s,i} + \beta_i^D}{\exp\left(\frac{2r_{s,i}}{\beta_i^D}\right) - 1} \right\| > 3\delta_{\max},$$

we can select $d_2 = d_4 = 3\delta_{\max}$, consequently follows that $d_1 = d_3$ has to be comprised between

$$d_1 > \left\| \frac{(r_{s,i} - \beta_i^D) \exp\left(\frac{2r_{s,i}}{\beta_i^D}\right) + r_{s,i} + \beta_i^D}{\exp\left(\frac{2r_{s,i}}{\beta_i^D}\right) - 1} \right\| - 3\delta_{\max}$$

and

$$d_1 < \left\| \frac{(r_{s,i} - \beta_i^D) \exp\left(\frac{2r_{s,i}}{\beta_i^D}\right) + r_{s,i} + \beta_i^D}{\exp\left(\frac{2r_{s,i}}{\beta_i^D}\right) - 1} \right\|.$$

Remark 2 (Forward Velocity). The values of β_i and $r_{s,i}$ clearly play a role on the modulus of the velocity of the i -th robot. By assuming to not having interactions with other robots, i.e., $\mathcal{A}_i \equiv \mathcal{S}_i$, we can analytically compute the distance of the i -th robot from the centroid $c_{\mathcal{A}_i}$ and hence the velocity, in fact by definition we have

$$\|p_i - c_{\mathcal{A}_i}\| = \left\| \frac{\int_{-r_{s,i}}^{r_{s,i}} z \exp\left(-\frac{|z - Kr_{s,i}|}{\beta_i}\right) dz}{\int_{-r_{s,i}}^{r_{s,i}} \exp\left(-\frac{|z - Kr_{s,i}|}{\beta_i}\right) dz} \right\|. \quad (13)$$

If $K \geq 1$ and $r_{s,i} > 0$, we obtain

$$\|p_i - c_{\mathcal{A}_i}\| = \left\| \frac{(r_{s,i} - \beta_i) \exp\left(\frac{2r_{s,i}}{\beta_i}\right) + r_{s,i} + \beta_i}{\exp\left(\frac{2r_{s,i}}{\beta_i}\right) - 1} \right\| \quad (14)$$

on the other hand when $0 < K < 1$ we have

$$\|p_i - c_{\mathcal{A}_i}\| = \left\| \frac{\rho_i \exp\left(\frac{r_{s,i}(K-1)}{\beta_i}\right) - \rho_i \exp\left(-\frac{r_{s,i}(K+1)}{\beta_i}\right) - 2Kr_{s,i}}{\exp\left(\frac{r_{s,i}(K-1)}{\beta_i}\right) + \exp\left(-\frac{r_{s,i}(K+1)}{\beta_i}\right) - 2} \right\|, \quad (15)$$

where $\rho_i = r_{s,i} + \beta_i$, by exploiting (3) and (13) we have a map between β_i and the i -th robot's velocity, in the case of non deformed cells, which may be regarded as standard operating conditions.

It is important to highlight that the centroid position remains unaffected by the value of K if $K > 1$, see (14). This implies that regardless of where the Laplacian function (7) is centered, as long as its mean value is at a distance greater than or equal to $r_{s,i}$, the centroid distance will only depend on β_i and $r_{s,i}$. On the other hand if $0 < K < 1$, it means that $\|p_i - e_i\| = Kr_{s,i} < r_{s,i}$, hence the centroid position has to depend on K , accordingly to (15). In light of these results, the velocity $\|\dot{p}_i\| = k_{p,i}\|p_i - c_{\mathcal{A}_i}\|$, in standard operating condition for the robot i , can be designed through $k_{p,i}$ or β_i^D .

Remark 3 (Pushing Effect). Another important insight is related to the pushing effect. According to Remark 2 the distance of the centroid from the robot does not depend on the mean value of the function $\varphi_i(q)$, if it is at a distance greater than $r_{s,i}$. This is true also if robots interact, in fact, by solving (10) it is clear that if $\beta_i > \beta_j$ then $\|p_i - c_{\mathcal{A}_i}\| < \|p_j - c_{\mathcal{A}_j}\|$, hence it results in a pushing effect, i.e., robot j will push robot i . In this scenario it is possible to compute analytically the equilibrium distance between robot i and robot j by solving

$$0 = \frac{d}{dt} \left\| \frac{\int_{-r_{s,i}}^{p_j(t)-p_i(t)-2\Delta_{ij}} z \exp\left(\frac{-|z-Kr_{s,i}|}{\beta_i}\right) dz}{\int_{-r_{s,i}}^{p_j(t)-p_i(t)-2\Delta_{ij}} \exp\left(\frac{-|z-Kr_{s,i}|}{\beta_i}\right) dz} \right\|.$$

By solving it for $p_j - p_i$, we compute the equilibrium distance d^* between robot i and j . Then the i -th robot velocity reads as follows:

$$\|\dot{p}_i\| = k_{p,i} \left\| \frac{\int_{-r_{s,i}}^{d^*-2\Delta_{ij}} z \exp\left(\frac{-|z-Kr_{s,i}|}{\beta_i}\right) dz}{\int_{-r_{s,i}}^{d^*-2\Delta_{ij}} \exp\left(\frac{-|z-Kr_{s,i}|}{\beta_i}\right) dz} \right\|.$$

Remark 4 (Numerical Simulations and Asynchrony). The simulations in Sec. IV are implemented in discrete time and with discretized cells \mathcal{A}_i , since computing the centroid position $c_{\mathcal{A}_i}$ in closed form it is not always possible. Notice that the computation of the centroid position $c_{\mathcal{A}_i}$ can be done in a distributed fashion. In fact each i -th robot, by relying on its position and encumbrance, and positions and encumbrances of the neighbors, can compute its cell \mathcal{A}_i . Once the cell geometry is defined each robot discretizes its own cell and assigns a weight to each point $q \in \mathcal{A}_i$, by means of $\varphi_i(q)$ (7). By approximating the integrals to compute the centroid positions with finite sums, each robot computes its centroid position $c_{\mathcal{A}_i}$. Because of this approximation, $\beta_{i,\min}$ has to be set together with the cell discretization dx . While $k_{p,i}$ has to be selected on the basis of the time discretization dt . In particular, to preserve safety and at the same time to allow the robots to generate the input asynchronously, we can verify that it is sufficient to have $k_{p,i}dt \leq \frac{\|p_i - c_{\mathcal{A}_i}\| - \delta_i}{\|p_i - c_{\mathcal{A}_i}\|}$, by rewriting in

the discrete form the equation (3). It means that by selecting $k_{p,i}dt = \frac{\|p_i - c_{\mathcal{A}_i}\| - \delta_i}{\|p_i - c_{\mathcal{A}_i}\|}$ the i -th robot reaches the position $p_i(t+1) = p_i(t) + \frac{\|p_i(t) - c_{\mathcal{A}_i}\| - \delta_i}{\|p_i(t) - c_{\mathcal{A}_i}\|} (p_i - c_{\mathcal{A}_i})$ in one single time step, which is a safe spot by construction, even if the position of the neighbors are not updated for one time step. Moreover, since $\|p_i - c_{\mathcal{A}_i}\| < r_{s,i}$, we can conclude that $k_{p,i}dt \leq 1 - \frac{\delta_i}{r_{s,i}}$. By considering dt equal to the computational time, this is not a strict assumption according to the computational time required by the algorithm (see Sec. IV-H). In the simulations in Sec. IV we selected $dx = 0.075$ (m), $dt = 0.033$ (s).

C. Learning policy with Lloyd-based support (LLB)

The choices behind the selection of β_i (8) and \bar{p}_i (9) are crucial to obtain acceptable performance and convergence. In the previous section we introduced a way to achieve convergence with acceptable performance. However, the selection of β_i (8) and \bar{p}_i (9) is far from optimal, i.e., a lower travel time can be achieved. Hence we propose to select these values by means of a learned function. By relying on learning-based techniques the convergence cannot be guaranteed anymore, but the safety is still ensured, both during training and testing, as it does not depend on β_i and \bar{p}_i . While prior works on learned navigation tasks require to properly shape the reward function to avoid collisions and at the same time to converge to the goal, our method allows to focus on learning how to reach the goal as quickly as possible.

Similarly to [61], we learn a high-level attention-based navigation policy that encodes the goal relative position and the relative positions and velocities of the other robots in the neighborhood (notice that the velocity is computed by relying on the past and actual positions). The learned latent representation is mapped to the parameters of a diagonal Gaussian distribution that we sample to obtain β_i and \bar{p}_i .

1) *RL Formulation*: Similarly to [53], the observation vector of each robot i is composed of its own information and relative states of all robots j within its sensing range:

$$\begin{aligned} s_i^t &= [\Delta p_{e,i}, \dot{p}_i, \delta_i, l_i], \\ s_j^t &= [\Delta p_{j,i}, \dot{p}_j, \delta_j], \quad \forall j \in \mathcal{N}_i, \end{aligned} \quad (16)$$

where s_i^t and s_j^t are the available information that robot i has of itself and other robots j in its sensing range. Notice that these information are obtained by relying on the onboard sensors. The relative positions of the goal and other robots are represented by $\Delta p_{e,i}$ and $\Delta p_{j,i}$. While the hyper-parameter l_i is initialized as $l_i = 0$, it becomes equal to 1 when $p_i \in \mathcal{B}(e_i, \varepsilon)$ and it stays equal to 1 until $p_i \notin \mathcal{B}(e_i, \varepsilon + d)$, where $d > 0$ is an arbitrary distance. All positions and velocities are represented in polar coordinates. We denote the joint observed state of all robots in \mathcal{N}_i by \mathcal{O}_i^t .

We seek to learn the optimal policy for each robot i : $\pi_i(s_i^t, \mathcal{O}_i^t)$, that maps its observation of the environment to an action vector: $a_i^t = (\Delta \bar{p}_i, \beta_i)$ with $\Delta \bar{p}_i = \bar{p}_i - p_i$, eventually guiding the robot towards its goal. Since placing \bar{p}_i beyond $r_{s,i}$ does not have any effect on $c_{\mathcal{A}_i}$ (see Remark 2), the action space is bounded by $\Delta \bar{p}_i \in \mathcal{B}(0, r_{s,i})$, while we constrained $\beta_i \in [0.1, 0.5]$.

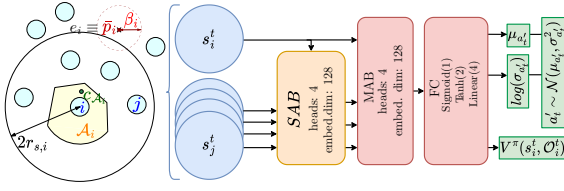


Figure 4: Overview of the learned policy network. The observed robots are encoded through a self-attention block (SAB) and decoded with a multi-headed attention block (MAB) and three fully connected layers (FC) that take s_i as query. The resulting vector is mapped to the parameters of the diagonal Gaussian distribution, $\mathcal{N}(\mu_{a'_i}, \sigma_{a'_i}^2)$, and value function estimate, $V^\pi(s_i^t, \mathcal{O}_i^t)$.

We design the reward function to motivate the ego-robot to reach and maintain its goal position while allowing other robots to reach theirs. The reward attributed to each robot W_i is defined as:

$$W_i(s_i^{t+1}, \mathcal{O}_i^{t+1}, a_i^t, s_i^t, \mathcal{O}_i^t) = W_{t,i} + W_{g,i}, \quad (17)$$

where $W_{t,i} = w_t - \Delta p_{e,i}$, and

$$W_{g,i} = \begin{cases} w_g & \text{if } l_i^{t+1} - l_i^t = 1 \\ 0 & \text{if } l_i^{t+1} - l_i^t = 0 \\ -w_g & \text{if } l_i^{t+1} - l_i^t = -1 \end{cases}$$

with $\Delta p_{e,i}$ being the increment of distance from robot i to its goal, and $w_g \in \mathbb{R}^+$ and $w_t \in \mathbb{R}^-$ being the reward for robot i achieving its goal, and the punishment for each time step that all robots have not achieved their goal, respectively. Note that there is no need for punishing collisions. Since the low-level controller always tracks the centroid of the cell, which now depends on the learned parameters $\bar{p}_i = p_i + \Delta \bar{p}_i$ and β_i , collisions cannot happen by definition. The episode ends when all the robots are within a distance ϵ of their goals or the time step limit has been reached.

2) *Policy Network Architecture:* Similar to [61] we learn a high-level attention-based policy that outputs the action vector $a'_i = (\Delta \bar{p}'_i, \beta'_i)$ conditioned to its observation of the environment. The architecture of the learned policy, shown in Figure 4 follows the encoder-decoder network paradigm [61], [68]. The available information of the environment (e.g., the goal and a variable number of agents inside the sensing range) is encoded through a self-attention block (SAB) that learns how each element's representation should be affected by the presence of others. Then a multi-headed attention block is used to pool the resulting latent representations conditioned to s_i^t . The resulting vector is then mapped through a fully connected layer FC to the parameters of a diagonal Gaussian distribution and an estimate of the state-value function. The diagonal Gaussian distribution is then sampled to obtain $a'_i = (\Delta \bar{p}'_i, \beta'_i)$, which is remapped to the action-space bounds. The state-value estimate is used only during training by the algorithm used to train the architecture. We employ the Proximal Policy Optimization (PPO) for training our neural network [69] with parameter-sharing. In our implementation [70], we utilize a combination of the surrogate loss and the KL-divergence term to ensure training stability. Additionally, an entropy regularization term

is integrated to foster exploration, as outlined in [71]. For a deeper dive into the algorithm's details, we direct readers to [69].

3) *Further considerations:* To guide and stabilize learned policy, we introduce a number of modifications both during training and testing. Firstly, to smooth our trajectories, we estimate a'_i by running an unbiased exponential recency-weighted average [72]:

$$\begin{aligned} a_i^{t+1} &= \frac{\alpha}{o^t} a'_i + (1 - \frac{\alpha}{o^t}) a_i^t \\ o^{t+1} &= o^t + \alpha(1 - o^t), \text{ with } o^0 = 0, \end{aligned} \quad (18)$$

where α is a hyperparameter that modulates how reactive is the policy to the output of the learned network. Secondly, we also assume that pushing effect (see Remark 3) is only necessary when the robot has not completed its tasks. Therefore, the output β'_i is clipped to the lower values $[0.1, 0.28]$ if $l_i = 1$, and it is clipped to the higher values $[0.32, 0.5]$ otherwise. These values are included in the range β_{\min} and β^D . A small gap between the lower values and the higher values is introduced in order to be sure to induce the pushing effect. This allows the robot to be more aggressive when the goal has not been achieved, and let other robots pass while it is close to its goal. We also substitute \bar{p}'_i by the goal position e_i when $l_i = 1$ to ensure stationary behavior when robots are at their goal, making the pushing effect easier to learn. We refer to the overall method as Learning Lloyd-based method (LLB). In the simulation results in Sec. IV, we show the advantages of LLB with respect to the pure learning method without the Lloyd-based support.

D. Dynamic constraints

Until now we only discussed the case of holonomic robots without constraints, however it is possible to implement the proposed algorithm also on unicycle, car-like robots, omnidirectional robots and aerial robots.

In fact, as we discussed, the holonomic robot has just to pursue a point position (i.e., the centroid $c_{\mathcal{A}_i}$). Similarly to [73], we use an MPC formulation to generate control inputs for the robots, which are compliant with the robot dynamics and that at each iteration generates a trajectory that remains inside the cell \mathcal{A}_i . In this way we can still guarantee safety at every time step. Each robot i solves the following MPC problem (we omit the i indexing to simplify the notation),

$$\min_{x_k, u_k} \sum_{k=0}^{N_t} J_k(x_k, u_k, c_{\mathcal{A}}), \quad (19a)$$

$$\text{s.t.: } x_k = f(x_{k-1}, u_{k-1}), \quad (19b)$$

$$x_k \in \mathcal{X}, u_k \in \mathcal{U}, \quad (19c)$$

$$p_k \in \mathcal{A}, \quad (19d)$$

$$x_0 = x_{\text{init}}, \quad (19e)$$

where k indicates the time index, N_t is the number of time instants in the MPC problem, J is the cost function, x_k and u_k are the state and inputs respectively, $f(x_{k-1}, u_{k-1})$ represents the robot dynamical constraints, $x_k \in \mathcal{X}$, $u_k \in \mathcal{U}$ are the state and input constraints respectively, and $x_0 = x_{\text{init}}$ is the initial

condition. The cost J can be chosen arbitrary as far as it incentives the tracking of the desired velocity. For each time instant k a possible formulation can be the following:

$$J_k = \left(v_k - v^D \frac{c_A - p_k}{\|c_A - p_k\|} \right)^\top \left(v_k - v^D \frac{c_A - p_k}{\|c_A - p_k\|} \right) + u_k^\top Q u_k, \quad (20)$$

where v_k is the robot's velocity in the x - y plane, v^D is the target absolute velocity that may be defined as a function of the distance from the centroid, i.e., $v^D = v^D(\|c_A - p_k\|)$ and Q is a positive definite matrix of weights.

It is important to note that since we have now introduced potentially complex robot dynamics (19b) as well as actuator and state constraints (19c), we do not guarantee the recursive feasibility of the MPC problem (19). In fact, the problem can be unfeasible if for example, the sensing range $r_{s,i}$ is too small and the robots have quite limited braking capability (in this case the constraints (19d) can be violated, compromising the safety of the system). However, in practice, for adequate sensing range and target velocity values, this is not an issue as is shown in Sec. V.

IV. SIMULATION RESULTS

The proposed approach is tested in simulation in several scenarios. We also provide a comparison with state of the art approaches. Through the numerical simulations we aim to further verify the scalability, the robustness, and the flexibility of the proposed approach. The multimedia material that accompanies the paper provides some videos of the simulation results. The source code can be found at <https://github.com/manuelboldrer/RBL>.

The parameters are selected as follows: $r_{s,i} = 1.5$ (m). Because of numerical issues due to the fact that the centroid position is not computed analytically but numerically, we also set a minimum value for $\beta_{i,\min} = 0.1$. Notice that the values for the parameters $d_1 = d_3, d_2 = d_4$ have to depend on $r_{s,i}$ and β_i^D for a correct convergence (see Proposition 1 and Remark 1). For the simulations we used $d_1 = d_3 = 0.1$ and $d_2 = d_4 = 3\delta_{\max}$ unless specified otherwise. Notice that, even if the chosen parameters may not always satisfy the sufficient conditions for convergence (depending on δ_i), we always obtained convergence from the simulation results. It indicates that the sufficient conditions provided for convergence are conservative, at least for scenarios that are not overly crowded (e.g., with $\eta < 0.1$).

The performance metrics that we considered include the maximum travel time (max time), which measures how much it takes to all the robots to converge towards their goal positions, the average speed of each robot during the mission (for each robot the mission stops when it reaches its goal position), and the robots success rate (RSR), computed as the ratio of robots that safely reached the goal to the total number of robots. The simulation results section is organized as follows: 1. we provide simulation results of RBL algorithm in crossing circle scenario, half crossing circle scenario and random room scenario. 2. We compared the proposed LLB approach with a pure learning algorithm without the Lloyd support and also with RBL. The comparison was done in

N	η	max time (s)	mean speed (m/s)	succ. rate
5	0.0061	5.18	3.96	1.00
10	0.0122	5.91	3.73	1.00
25	0.0306	7.98	2.91	1.00
50	0.0612	11.09	2.40	1.00
300	0.0133	30.76	1.52	1.00

Table I: Circle crossing: quantitative data form the simulation in Figure 5.

multiple scenarios by repeating each experiment 20 times to have a statistical evidence. 3. We provide simulation results of RBL algorithm by testing different dynamical constraints, i.e., unicycle and car-like. 4. To test the robustness and reliability of RBL we added randomness in the selection of robot encumbrance δ_i , β^D and $k_{p,i}$ and we run 100 simulations by accounting also different number of robots in the scene. 5. We provide a comparison with the state of the art. In particular we compared RBL by considering the unicycle case with LB [60] and RL-RVO [47], which performs better than SARL [54], GA3C-CADRL [55] and NH-ORCA [6]. Then we compared RBL in the holonomic case with RVO2 [74], SBC [15], GCBF+ [75], BVC [28], DMPC [76] and LCS [77]. 5. Finally, we provided some insights on the computational cost of the proposed algorithm.

A. Crossing circle (RBL)

We report several simulations in the crossing circle scenario. In Fig. 5 we depicted the trajectories obtained by considering $N = [5, 10, 25, 50, 300]$ homogeneous holonomic robots. The radius of the circle is $R_c = [10, 10, 10, 10, 15]$ (m). The value of $\beta_i^D = 0.5, \forall i = 1, \dots, N$. The robot encumbrance $\delta_i = [0.35, 0.35, 0.35, 0.35, 0.1]$ (m), and $k_{p,i} = 6, \forall i = 1, \dots, N$.

In Table I we report the quantitative results, where N is the number of robots and $\eta = \frac{\text{Area}_{\text{robots}}}{\text{Area}_{\text{tot}}}$ is what we called the *crowdness factor*, which is the ratio between the sum of the area occupied by the robots and the total mission space area, it is an indicator of the challenging and intricate nature of the considered scenario.

In Figure 6 we show other two simulations, where we picked a random encumbrance radius for each robot $\delta_i \in [0.1, 0.5]$. On the left hand side we selected $\beta_i^D = 0.5, \forall i = 1, \dots, N$, while on the simulation on the right hand side we selected $\beta_i^D \in [0.2, 1.5]$ randomly for each robot. Figure 7 shows the effects of the choice of β^D on the travel time for each robot, in accordance with Remark 2, by increasing β^D the travel time increases as well.

B. Half crossing circle (RBL)

Similarly to the crossing circle case, we report some simulations for the half crossing circle scenario. In this case, the goal position for each robot is shifted by an angle of $\pi + \gamma$, rather than being exactly out of phase by π . In Figure 8, we show that even if the robots follow the right hand side rule according to (9), our algorithm can also manage this challenging situations, where the emergent behavior is a clockwise rotation. In Table II we report the quantitative results.

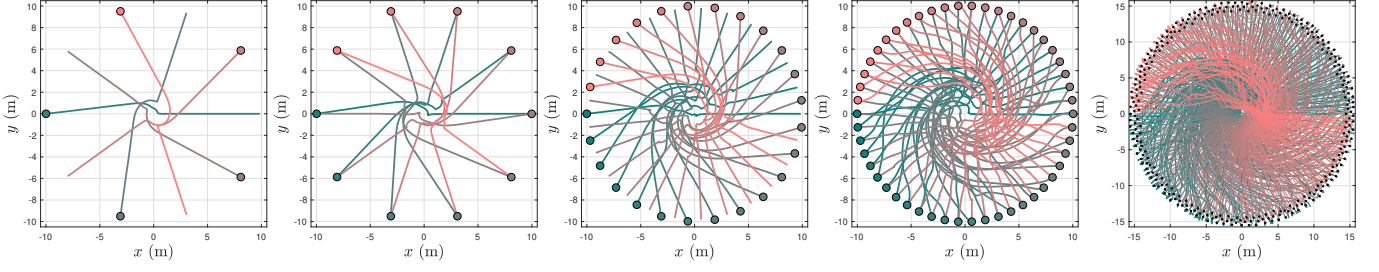


Figure 5: Circle crossing: simulation results with $N = [5, 10, 25, 50, 300]$ holonomic robots. The value $\beta^D = 0.5$ is the same for all the robots.

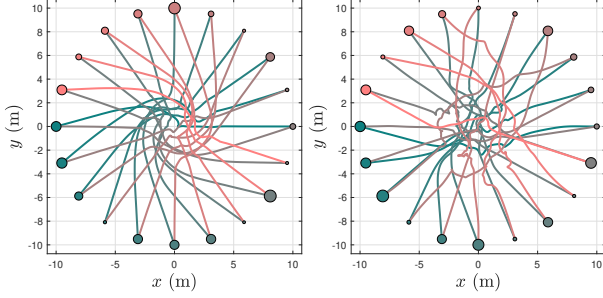


Figure 6: Circle crossing: simulation results with $N = 20$ holonomic robots with random encumbrance r . On the left hand side $\beta_i^D = 0.5$ for all the robots, On the right hand side β_i^D is random and different from robot to robot.

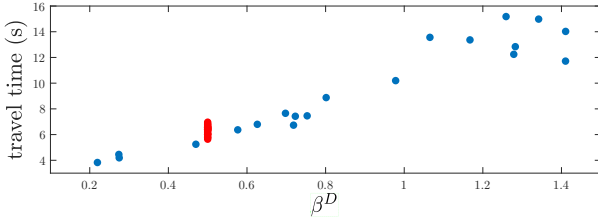


Figure 7: Dependence of the travel time with respect to β_i^D . Each dot represents the performance of one robot. In red the left hand side simulation in Figure 6, in blue the right hand side simulation in Figure 6.

C. Random room (RBL)

In this scenario we report two simulations. The initial location and the final goal location are selected randomly. In Figure 9, on the left hand side, $\eta_1 = 0.157$ and $N = 20$ homogeneous robots, on the right hand side $\eta_2 = 0.135$ and $N = 300$ heterogeneous (random size) robots. In both cases the robots successfully converge to a neighborhood of the goal positions.

D. Learning approach (LLB)

We implemented the Learning Lloyd-based (LLB) algorithm introduced in Section III-C, to verify the effectiveness of using a Lloyd-based support on learning-based algorithms. In Table III we compared the same learning algorithm, with the Lloyd support (LLB), without the support of the LB algorithm (we indicated it in Table III as Pure Learning algorithm), and also with the RBL algorithm.

N	η	max time (s)	mean speed (m/s)	succ. rate
5	0.0061	5.05	3.95	1.00
10	0.0122	5.44	3.77	1.00
25	0.0306	6.47	3.43	1.00
50	0.0612	7.01	2.76	1.00
300	0.0133	16.59	1.91	1.00

Table II: Half circle crossing: quantitative data form the simulation in Fig. 8.

We made few changes to train the learning approach without Lloyd support. In fact in this case, we only learn a point relative to the robot $\Delta \bar{p}_i \in \mathcal{B}(0, r_{s,i})$, to follow with velocity $\dot{p}_i = v_{i,\max} \frac{\Delta \bar{p}_i}{r_{s,i}}$. Since collisions under this policy are possible, additional reward signal r_{coll} is also added to the reward function to punish collision events. All other conditions have been maintained. We observed that the addition of LB during training simplifies the problem. Pure learning method requires trading off collision avoidance with fast goal convergence. Instead, adding the safety LB layer during training allows to only consider fast convergence towards the goal. We run multiple simulations in different scenarios. It results that the LLB was able to achieve a success rate of 1.00, while pure learning presents failures even in simple scenarios (e.g., with $N = 5$). With respect to RBL, the LLB performs better in symmetric scenarios (i.e., circle scenarios) and slightly worse in the random room scenarios. In the case of symmetric scenarios this is due to the fact that RBL needs some time to break perfect symmetries by engaging the right hand rules (the transient time depends on the parameters settings), while LLB is able to break symmetries immediately as can be seen from Figure 10. In the figure we depict the trajectories obtained from LLB in the crossing circle scenarios reported also in Table III.

E. Dynamical constraints (RBL)

We also tested our algorithm with different dynamical models, i.e., the unicycle and the car-like. In Figure 11 we depicted the results in the crossing circle scenario for $N = [5, 10, 25]$, for the unicycle model (top) and for the car-like model (bottom). In both cases we set a maximum and desired forward velocity $v^D = 1.5$ (m/s). The quantitative results are reported in Tables IV and V.

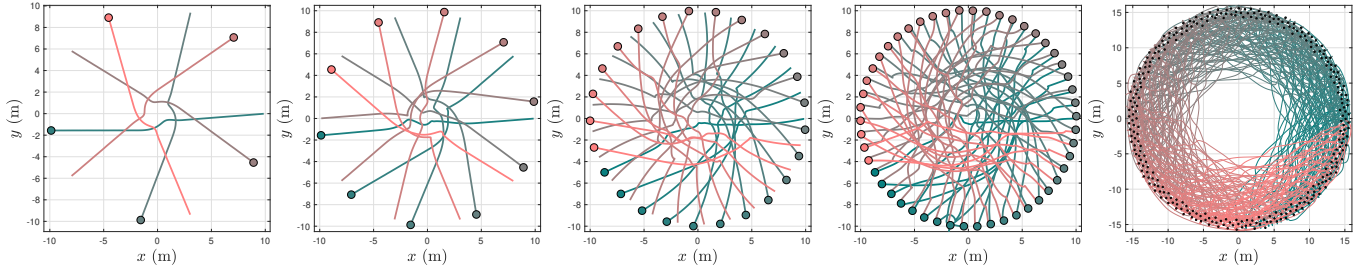


Figure 8: Half circle crossing: simulation results with $N = [5, 10, 25, 50, 300]$, holonomic robots. The value $\beta^D = 0.5$ is the same for all the robots. The goal position is rotated with respect to the crossing scenario of a value $\gamma = [\pi/20, \pi/20, \pi/6, \pi/6, \pi/2]$.

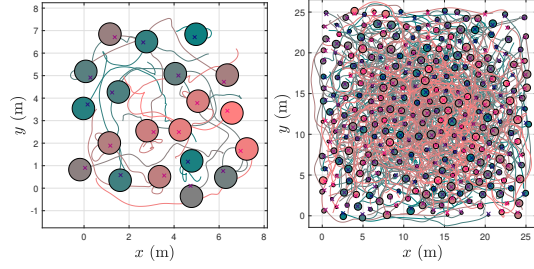


Figure 9: (left) Room 7x7 (m²): simulation results with $N = 20$ holonomic robots with crowding factor $\eta = 0.157$. (right) Room 25x25 (m²): simulation results with $N = 300$ holonomic robots with crowding factor $\eta = 0.135$ and random encumbrance δ .

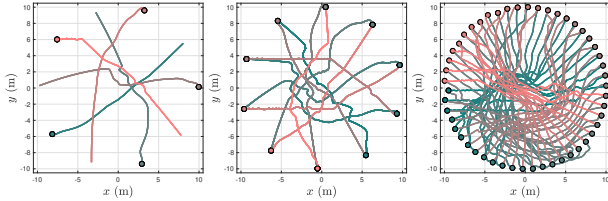


Figure 10: Crossing circle: simulation results with $N = [5, 10, 50]$ holonomic robots, by using LLB approach.

RBL	N	η	max time (s)	succ. rate
circle (10 m)	5	0.0045	6.56	1.00
room (9 × 9 m ²)	5	0.0289	2.25	1.00
circle (10 m)	10	0.0090	7.78	1.00
room (9 × 9 m ²)	10	0.0349	2.74	1.00
circle (10 m)	50	0.0450	17.65	1.00
room (15 × 15 m ²)	50	0.0628	12.36	1.00
Pure Learning	N	η	max time (s)	succ. rate
circle (10 m)	5	0.0045	5.25	0.94
room (9 × 9 m ²)	5	0.0289	2.79	0.56
circle (10 m)	10	0.0090	6.38	0.77
room (9 × 9 m ²)	10	0.0349	3.31	0.04
circle (10 m)	50	0.0450	-	0.00
room (15 × 15 m ²)	50	0.0628	-	0.00
LLB	N	η	max time (s)	succ. rate
circle (10 m)	5	0.0045	5.47	1.00
room (9 × 9 m ²)	5	0.0289	2.42	1.00
circle (10 m)	10	0.0090	6.43	1.00
room (9 × 9 m ²)	10	0.0349	3.37	1.00
circle (10 m)	50	0.0450	13.35	1.00
room (15 × 15 m ²)	50	0.0628	13.67	1.00

Table III: Simulation results for rule-based Lloyd (RBL), Pure Learning and Learning with Lloyd support (LLB). We considered $N = [5, 10, 50]$ holonomic robots in the crossing circle scenario and in the random room scenario, with robot encumbrance $\delta_i = 0.3$ (m). The maximum time is an average of the successful simulations.

F. Robustness and reliability (RBL)

For the crossing circle and random room in the holonomic case we run additional simulations to test the robustness of the algorithm to the change in parameters. According to the data reported in [50] Sec. 5.4, it is clear that in learning-based solutions performance, safety and convergence degrade by changing parameters such as the dimension of the robots and the desired velocity. In the following we show an analysis of robustness by considering a heterogeneous scenario and by selecting randomly the encumbrances of the robots $\delta_i \in [0.1, 0.5]$, the value of $\beta_i^D \in [0.2, 0.75]$ and $k_{p,i} \in [3, 6]$. We run 100 simulations with $N = [20, 40, 100]$ robots. The simulation results are reported in Table VI, the success rate is always equal to 1.00.

G. Comparison with state of the art

As we already mentioned, our main advantages with respect to the algorithms proposed in the literature reside in the combination of four aspects:

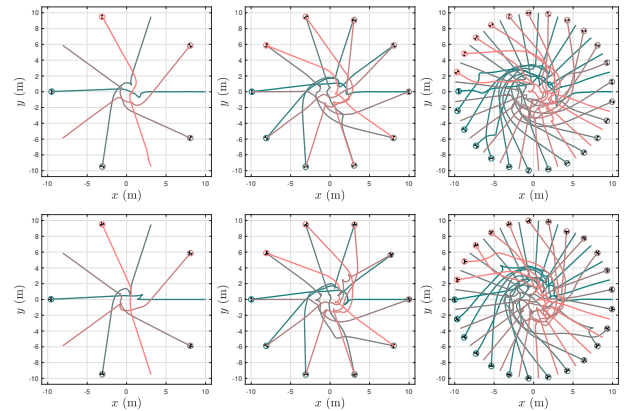


Figure 11: Crossing circle: simulation results with $N = [5, 10, 25]$ non-holonomic robots. At the top the unicycle model, at the bottom the car-like model.

N	η	max time (s)	mean speed (m/s)	succ. rate
5	0.006125	21.50	1.09	1.00
10	0.01225	26.60	1.01	1.00
25	0.0306	32.90	0.82	1.00

Table IV: Circle crossing unicycles: quantitative data from the simulation in Fig. 11 (top).

N	η	max time (s)	mean speed (m/s)	succ. rate
5	0.006125	26.90	0.86	1.00
10	0.01225	32.00	0.80	1.00
25	0.0306	44.40	0.64	1.00

Table V: Circle crossing car-like: quantitative data from the simulation in Fig. 11 (bottom).

1. We can achieve success rate of 1.00 in very crowded scenarios. 2. Each robot needs to know only its position p_i , its encumbrance δ_i , its goal position e_i , its neighbours' positions p_j and encumbrance δ_j (if $\|p_i - p_j\| \leq 2r_{s,i}$, then $j \in \mathcal{N}_i$); 3. The control inputs for each robot can be generated in an asynchronous fashion without affecting safety and convergence. 4. We can account for heterogeneous conditions, i.e., different robots' encumbrances and different robots' dynamics and velocities;

The combination of these features are not provided by any other algorithm in the literature. In the following, we provide a comparison with some state of the art algorithms.

Firstly, we considered the non-holonomic (unicycle) case, we compared the performance of our rule-based Lloyd algorithm (RBL) with LB [60] and RL-RVO [47], which demonstrates superior performance and success rate compared to other algorithms such as SARL [54], GA3C-CADRL [55], NH-ORCA [6].

We considered the crossing circle scenario $R_c = 4$ (m) with $N = [6, 20, 30, 100]$, $\delta_i = 0.2$ (m) ($\delta_i = 0.1$ (m) for $N = 100$), a maximum forward velocity $v_{i,\max} = 1.5$ (m/s), and limits on the accelerations of $a_{i,\max} = 1$ (m/s²). As a result (see Table VIII), RBL executes better in terms of success rate with respect to the other algorithms (in this case the success rate is the ratio between the number of missions where the robots converged safely and the total number of missions simulated). On the other hand, when it succeeds, RL-RVO has on average better performance. This is also due to the fact that RL-RVO relies on stronger assumptions (each robot has to collect exteroceptive observations).

We also propose a comparison with other *reactive* algorithms for the holonomic robots case, such as RVO2 [74],

RBL	N	mean of η	max time (s)	mean speed (m/s)	RSR
circle (4 m)	20	0.112	8.87 ± 0.98	1.70 ± 0.10	1.00
room (7×7 m ²)	20	0.115	5.33 ± 1.13	1.79 ± 0.25	1.00
circle (7 m)	40	0.073	12.96 ± 0.84	1.80 ± 0.11	1.00
room (9×9 m ²)	40	0.139	10.24 ± 2.16	1.46 ± 0.07	1.00
circle (16 m)	100	0.0352	24.57 ± 1.15	2.03 ± 0.10	1.00
room (15×15 m ²)	100	0.125	21.83 ± 4.89	1.46 ± 0.07	1.00

Table VI: Simulation results for $N = [20, 40, 100]$ robots in the crossing circle scenario and in the random room scenario, with $\delta_i \in [0.1, 0.5]$ (m), $\beta_i^D \in [0.2, 0.75]$ and $k_{p,i} \in [3, 6]$.

	N	η	max time (s)	mean speed (m/s)	succ. rate
SBC [15]	5	0.00253	42.70	0.131	1.00
	10	0.00506	45.96	0.125	1.00
	20	0.0101	56.33	0.118	1.00
	50	0.0252	71.08	0.106	1.00
	N	η	max time (s)	mean speed (m/s)	succ. rate
RBL (ours)	5	0.00253	29.79	0.195	1.00
	10	0.00506	32.17	0.192	1.00
	20	0.0101	39.46	0.185	1.00
	50	0.0252	49.36	0.180	1.00

Table VII: Circle crossing: quantitative data with unicycle model. We compared our method (RBL) with SBC [15].

SBC [15], GCBF+ [75] and also with recent *predictive planning* methods such as BVC [28], [30], DMPC [76] and LCS [77]. Even if some of these algorithms may have better performance in terms of time to reach the goal in certain scenarios, they lack of guarantees of live-lock and deadlock avoidance, hence, even in simple scenarios they may fail the mission. In [77] (Sec. IV, Fig. 5) it is clear that the success rate of the mission decreases considerably for $N > 50$, as well for BVC, DMPC and LCS. Also RVO2 [74] presents deadlock issues in symmetric conditions (crossing circle) and in crowded random room scenarios with high crowdness factor, e.g., we tested a random room scenario with $\eta = 0.452$, it results in a SR = 0.65. For the SBC approach [15], in Sec. VII, it is clearly stated that the algorithm suffers of what they called type III deadlock and live-lock as well. We tested it in a scenario with $\eta = 0.452$, it results in SR = 0.00. We obtain the same SR = 0.00 for more advanced variants such as GCBF+ [75]. While in the same scenario our RBL reached SR = 1.00. Finally, for SBC we also provided a comparison of the performance in simple crossing circle scenarios with $N = [5, 10, 20, 50]$ (see Table VII). Since SBC performance may vary on the basis of the parameter tuning, we considered the provided scenario, where robots encumbrance $\delta_i = 0.0675$ (m), and maximum velocity $v_{i,\max} = 0.2$ (m/s) and we compared it with our method in the same conditions. Contrary to other methods seen before, this can be considered a fair comparison, since SBC does not use exteroceptive information as our method. In this case, RBL performs better also in terms of time to reach the goals.

In conclusion, with respect to the state of the art, our RBL algorithm often achieves similar performance in terms of time to reach the goal, nevertheless it consistently attains a success rate of 1.00, and it does so without relying on exteroceptive observations (e.g., future intentions of the other robots), the neighbours velocities, or synchronization between the robots. For the best of our knowledge, this is not provided by any other distributed algorithm in the literature. In this section we provided a relevant amount of comparisons with state of the art algorithms (including also the ones that uses exteroceptive observation). The main result that we obtained can be synthesized as follows: our algorithm outperforms all the tested algorithms in terms of success rate, i.e., we always obtained SR = 1.00 in all the tested scenarios, while LB, RL-RVO, SARL, GA3C-CADRL, NH-ORCA, RVO2, SBC, BVC, GCBF+, DMPC, and LCS obtained a SR < 1.00.

	N	η	max time (s)	mean speed (m/s)	succ. rate
RL-RVO [47]	6	0.015	7.10	1.19	1.00
	20	0.05	13.84	0.73	0.71
	30	0.075	21.89	0.62	0.10
	100	0.0625	-	-	0.00
	N	η	max time (s)	mean speed (m/s)	succ. rate
LB [60]	6	0.015	13.42	0.66	1.00
	20	0.05	-	-	0.00
	30	0.075	-	-	0.00
	100	0.0625	-	-	0.00
	N	η	max time (s)	mean speed (m/s)	succ. rate
RBL (ours)	6	0.015	9.86	0.89	1.00
	20	0.05	17.85	0.65	1.00
	30	0.075	26.16	0.59	1.00
	100	0.0625	28.76	0.39	1.00

Table VIII: Circle crossing: quantitative data with unicycle model. We compared our method (RBL) with LB [60] and RL-RVO [47] method, since SARL [54], GA3C-CADRL [55] and NH-ORCA [6] underperform it according to [47] (Table II). Notice that in RL-RVO, each robot has to collect exteroceptive observations, i.e., the method relies on a communication network.

We want to underline that if a reliable communication network and a good computational power are available, then IMPC-DR [40] and ASAP [41] are valid solutions that provide a success rate of $SR = 1.00$ similarly as our.

H. Computational time

The computational time of the proposed approach depends mainly on $r_{s,i}$ (assuming a fixed space discretization step $dx = 0.075$ (m)), since we compute the centroid position numerically. We tested the algorithm in Python on an AMD Ryzen 7 5800H. By considering that $r_{s,i}$ should be limited to a maximum amount of 2 (m) (notice that $r_{s,i}$ is half the sensing radius capability) a real-time implementation is largely feasible. In fact we measured for $r_{s,i} = 2.0$ (m) an average computational time of $t_c = 10$ (ms), for $r_{s,i} = 1.5$ (m) we measured $t_c = 5.5$ (ms), while for $r_{s,i} = 1.0$ (m) the computational time reduces to $t_c = 2$ (ms). The addition of the MPC to account for dynamic constraints has an impact on the computational time. However, despite a clear increase in the computational time, it does not prevent to be used for real-time applications (as it is shown in the experimental result Sec. V). We measured an increase of 16 (ms) on average.

V. EXPERIMENTAL RESULTS

We tested our RBL algorithm on different robotic platforms. In particular, car-like robots, unicycle robots, omnidirectional robots, and aerial robots. Notice that in the following implementations we relied on a communication network to share the neighbors' positions and encumbrances. Nevertheless, by means of onboard sensors such as lidars, cameras or uvdar [78], the neighbors' positions can be easily inferred (Assumption 1), hence the functioning of the algorithm would be comparable (or better since less delays are introduced) in the absence of a communication network. In the car-like case, we used $N = 3$ scaled-down car-like robots with $\delta_i = 0.2$ (m), the robots consist of a modified Waveshare JetRacer Pro AI kit. We selected $r_{s,i} = 1.5$ (m), $\beta^D = 0.5$, $d_1 = d_3 = 0.15$ and, $d_2 = d_4 = 0.45$. In the following, we report the results

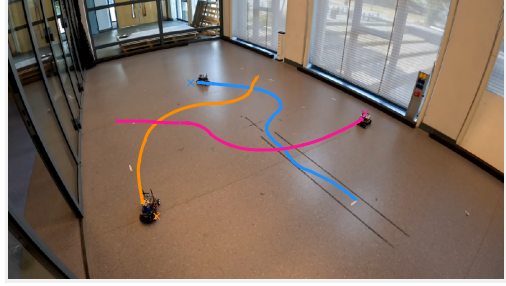


Figure 12: Experiments with $N = 3$ car-like robots in a crossing circle scenario.

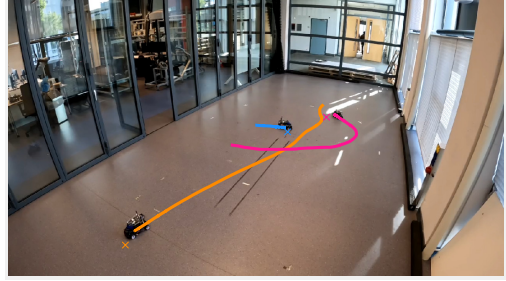


Figure 13: Experiments with $N = 3$ car-like robots in a random room scenario.

obtained from a crossing circle scenario and a random room scenario with $N = 3$. In both the scenarios the robots converge safely to their goal positions, in accordance with the theory and the simulation results. The dynamic constraint (19b) is now described as the following kinematic bicycle model:

$$\begin{bmatrix} \dot{x} \\ \dot{y} \\ \dot{\eta} \\ \dot{v} \end{bmatrix} = \begin{bmatrix} v \cos \eta \\ v \sin \eta \\ \frac{v \tan(\delta)}{l} \\ h(\tau, v) \end{bmatrix},$$

where x, y, η, v are respectively the x and y position of the rear axle, the orientation of the robot and the longitudinal velocity, l is the length of the robot, τ and δ are the throttle and steering angle inputs, while $h(\tau, v)$ is the motor characteristic curve. Figs. 12 and 13 report two experiments in the crossing circle and random room scenarios, respectively. We depicted with solid lines the trajectories followed by the robots and with crosses the goal locations. The robots safely converged to their goal locations. In Table IX we report the quantitative data.

For the unicycle robots case, we used $N = 3$ Clearpath Jackals with $\delta_i = 0.3$ (m), $\beta^D = 0.5$, $d_1 = d_3 = 0.15$, and $d_2 = d_4 = 0.9$. Also in this case, we report the results obtained from a crossing circle scenario and a random room scenario with $N = 3$. Again, the robots converge safely to

RBL	N	η	max time (s)	mean speed (m/s)	RSR
circle (1.5 m)	3	0.0075	7.69	0.428	1.00
room (5×3 m ²)	3	0.014	9.50	0.448	1.00

Table IX: Quantitative experimental results for $N = 3$ car-like robots in the crossing circle scenario and in the random room scenario with $v^D = 0.5$ (m/s) (see Figure 12 and 13).

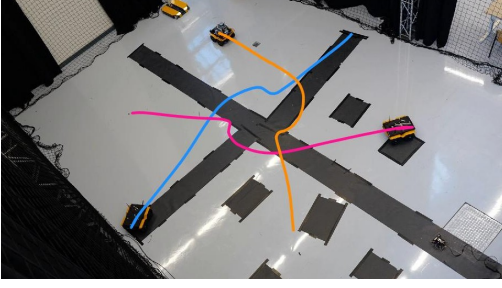


Figure 14: Experiments with $N = 3$ unicycle-like robots in a crossing circle scenario.

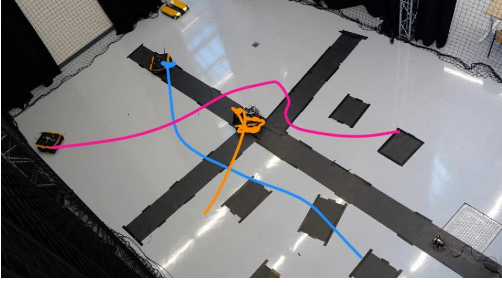


Figure 15: Experiments with $N = 3$ unicycle-like robots in a random room scenario.

their goal locations. In this case the dynamic constraint (19b) can be written as:

$$\begin{bmatrix} \dot{x} \\ \dot{y} \\ \dot{\theta} \end{bmatrix} = \begin{bmatrix} v \cos \eta \\ v \sin \eta \\ \omega \end{bmatrix},$$

where x, y, θ, v, ω are respectively the x and y position of the rear axle, the orientation of the robot, the longitudinal and the angular velocities. Figs. 14 and 15 report two experiments in the crossing circle and random room scenarios, respectively. In Table X we report the quantitative data.

We also report three experiments with heterogenous agents. In particular, in Figure 16 we considered the case of $N = 4$ robots with three Clearpath Jackals and one Clearpath Dingo. The Clearpath Dingo is an omnidirectional robot hence it can directly take as control inputs the velocities \dot{p}_i . In Figure 17, we considered the case of $N = 5$ agents, with three Clearpath Jackals, one Clearpath Dingo and one Human being. In this case the human being is seen by the robots as another robot, hence the algorithm does not change. The only difference lies in the human being motion, which does not follow the RBL control law. Nevertheless, the robots avoided collisions and achieved their goal locations. Finally, in Figure 18, we reported the obtained paths by using $N = 7$ aerial robots (four DJI F450 and three Holybro X500 [79], [80]) in the crossing circle

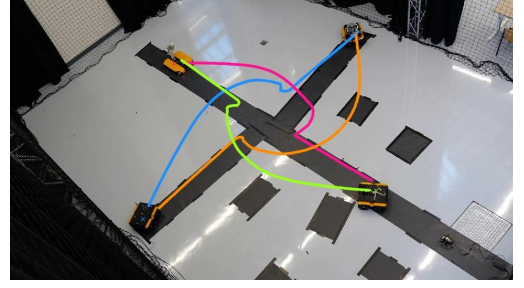


Figure 16: Experiments with $N = 4$ robots, three unicycle-like robots and one holonomic robot in a crossing circle scenario.

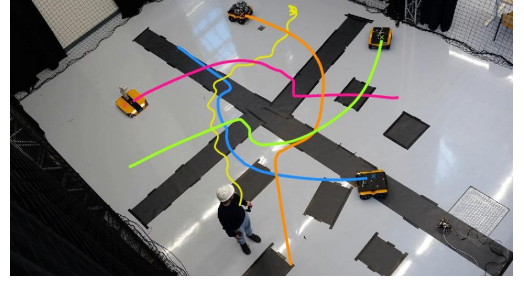


Figure 17: Experiments with $N = 5$ agents, three unicycle-like robots, one holonomic robot and one human being in a crossing circle scenario.

scenario. In this case, we considered $\delta_i = 2.50$ (m), $r_{s,i} = 3.0$ (m), $d_1 = d_3 = 0.2$, $d_2 = d_4 = 1.0$, $\beta_i^D = 1.5$ and $\eta = 0.194$. To reach the centroid positions, we relied on the MRS UAV system [81]. For the localization the robots relied on GPS. Even in the presence of uncertainties, tracking errors, and imperfect communication, each robot satisfied $p_k \in \mathcal{A}$ at every time step, and the robots safely converged to their goal regions. In Fig. 19 we depicted the distances as a function of time, notice that the robots reach their goal region without exceeding the safe minimum distance, which is set to $2\delta_i = 5$ (m). Videos of the experiments are provided in the multimedia material.

VI. CONCLUSIONS

This paper provided two solutions for multi-robot motion planning and control, namely rule-based Lloyd (RBL) and Learning Lloyd-based (LLB) algorithm. Our solutions prove beneficial in a settings lacking of a centralized computational unit or a dependable communication network. In the case of RBL, we demonstrated both theoretically and through a comprehensive simulation campaign that each robot safely converges to its goal region. While through LLB, we showed that the Lloyd-based algorithm can be used as a safety-layer for learning-based algorithms. We believe that it can pave the way towards safe guaranteed learning-based algorithms and online learning as well. We provided also experimental results for RBL approach with car-like robots, unicycle robots, omnidirectional robots, and aerial robots on the field.

The main limitations of the proposed approach are the following: we can only guarantee to converge in a proximity of the goal position (see Proposition 1), the parameters have to be chosen carefully to meet the requirements for guarantee

RBL	N	η	max time (s)	mean speed (m/s)	RSR
circle (3 m)	3	0.030	16.90	0.415	1.00
room (7×4 m ²)	3	0.010	21.90	0.442	1.00

Table X: Quantitative experimental results for $N = 3$ unicycle-like robots in the crossing circle scenario and in the random room scenario $v^D = 0.5$ (m/s) (see Figure 12 and 13).

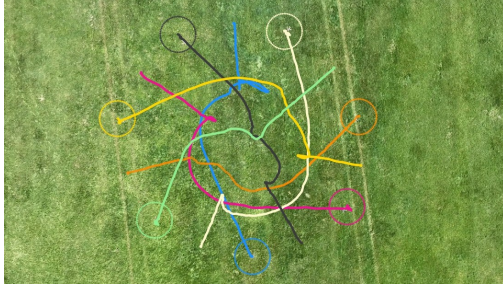


Figure 18: Experiment with $N = 7$ aerial robots in a crossing circle scenario, the colored circles of radius $\delta_i = 2.5$ (m) indicate the final positions of the aerial robots.

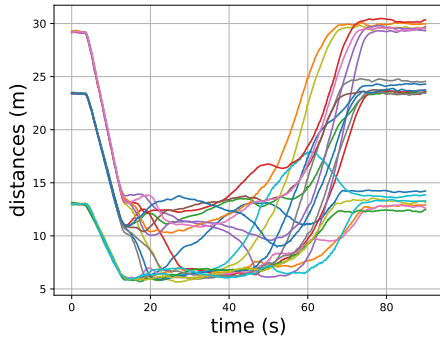


Figure 19: Experiments with $N = 7$ aerial robots, distances between robots as a function of time.

convergence (see Remark 1), even if we provided a rigorous way to select most of them, a tuning process is necessary in order to impose the desired behavior to the robot motion (e.g., more aggressive or more conservative), the weight matrix Q in the MPC cost function (20) have to be carefully chosen in order to obtain the desired behavior. Finally, we have to be aware that the numerical simulations give an approximation of the centroid position. To obtain a better approximation we have to pay in computational efficiency (by decreasing dx).

In the future, our objectives include addressing some of the mentioned limitations, i.e., obtaining a closed form solution for the centroid position, and design an adaptive law for the d_2 parameter in (8) to converge to the goal position. We plan to do experiments in scenarios that include multiple non-cooperative or partially-cooperative agents in the mission space (i.e., multiple human beings). We plan to do the experiments relying only on onboard sensors to extrapolate the neighbors' positions. Finally, we plan to further develop the LLB algorithm by testing the benefits of the LB layer during training on other learning-based algorithms, and by synthesizing hybrid solutions with RBL to provide guarantees of convergence.

REFERENCES

- [1] G. Sharon, R. Stern, A. Felner, and N. R. Sturtevant, "Conflict-based search for optimal multi-agent pathfinding," *Artificial Intelligence*, vol. 219, pp. 40–66, 2015.
- [2] J. Li, A. Tinka, S. Kiesel, J. W. Durham, T. S. Kumar, and S. Koenig, "Lifelong multi-agent path finding in large-scale warehouses," in *Proceedings of the AAAI Conference on Artificial Intelligence*, vol. 35, no. 13, 2021, pp. 11 272–11 281.
- [3] J. Cheng, H. Cheng, M. Q.-H. Meng, and H. Zhang, "Autonomous navigation by mobile robots in human environments: A survey," in *2018 IEEE international conference on robotics and biomimetics (ROBIO)*. IEEE, 2018, pp. 1981–1986.
- [4] J. Van den Berg, M. Lin, and D. Manocha, "Reciprocal velocity obstacles for real-time multi-agent navigation," in *2008 IEEE international conference on robotics and automation*. Ieee, 2008, pp. 1928–1935.
- [5] J. Van Den Berg, S. J. Guy, M. Lin, and D. Manocha, "Reciprocal n-body collision avoidance," in *Robotics Research: The 14th International Symposium ISRR*. Springer, 2011, pp. 3–19.
- [6] J. Alonso-Mora, A. Breitenmoser, M. Ruffi, P. Beardsley, and R. Siegwart, "Optimal reciprocal collision avoidance for multiple non-holonomic robots," in *Distributed Autonomous Robotic Systems: The 10th International Symposium*. Springer, 2013, pp. 203–216.
- [7] M. Boldrer, L. Palopoli, and D. Fontanelli, "Socially-aware multi-agent velocity obstacle based navigation for nonholonomic vehicles," in *2020 IEEE 44th Annual Computers, Software, and Applications Conference (COMPSAC)*. IEEE, 2020, pp. 18–25.
- [8] S. H. Arul and D. Manocha, "V-rvo: Decentralized multi-agent collision avoidance using voronoi diagrams and reciprocal velocity obstacles," in *2021 IEEE/RSJ International Conference on Intelligent Robots and Systems (IROS)*. IEEE, 2021, pp. 8097–8104.
- [9] J. Godoy, S. J. Guy, M. Gini, and I. Karamouzas, "C-nav: Distributed coordination in crowded multi-agent navigation," *Robotics and Autonomous Systems*, vol. 133, p. 103631, 2020.
- [10] A. Giese, D. Latypov, and N. M. Amato, "Reciprocally-rotating velocity obstacles," in *2014 IEEE International Conference on Robotics and Automation (ICRA)*. IEEE, 2014, pp. 3234–3241.
- [11] R. Zheng and S. Li, "Mcca: A decentralized method for collision and deadlock avoidance with nonholonomic robots," *IEEE Robotics and Automation Letters*, 2024.
- [12] D. Helbing and P. Molnar, "Social force model for pedestrian dynamics," *Physical review E*, vol. 51, no. 5, p. 4282, 1995.
- [13] M. Boldrer, M. Andreetto, S. Divan, L. Palopoli, and D. Fontanelli, "Socially-aware reactive obstacle avoidance strategy based on limit cycle," *IEEE Robotics and Autom. Lett.*, vol. 5, no. 2, pp. 3251–3258, 2020.
- [14] R. Gayle, W. Moss, M. C. Lin, and D. Manocha, "Multi-robot coordination using generalized social potential fields," in *International Conference on Robotics and Automation*. IEEE, 2009, pp. 106–113.
- [15] L. Wang, A. D. Ames, and M. Egerstedt, "Safety barrier certificates for collisions-free multirobot systems," *IEEE Transactions on Robotics*, vol. 33, no. 3, pp. 661–674, 2017.
- [16] F. Celi, L. Wang, L. Pallottino, and M. Egerstedt, "Deconfliction of motion paths with traffic inspired rules," *IEEE Robotics and Automation Letters*, vol. 4, no. 2, pp. 2227–2234, 2019.
- [17] X. Zhou, J. Zhu, H. Zhou, C. Xu, and F. Gao, "Ego-swarm: A fully autonomous and decentralized quadrotor swarm system in cluttered environments," in *2021 IEEE international conference on robotics and automation (ICRA)*. IEEE, 2021, pp. 4101–4107.
- [18] D. Fox, W. Burgard, and S. Thrun, "The dynamic window approach to collision avoidance," *IEEE Robotics & Automation Magazine*, vol. 4, no. 1, pp. 23–33, 1997.
- [19] L. Ferranti, L. Lyons, R. R. Negenborn, T. Keviczky, and J. Alonso-Mora, "Distributed nonlinear trajectory optimization for multi-robot motion planning," *IEEE Transactions on Control Systems Technology*, vol. 31, no. 2, pp. 809–824, 2022.
- [20] A. Tajbakhsh, L. T. Biegler, and A. M. Johnson, "Conflict-based model predictive control for scalable multi-robot motion planning," in *2024 IEEE International Conference on Robotics and Automation (ICRA)*. IEEE, 2024, pp. 14 562–14 568.
- [21] H. Zhu and J. Alonso-Mora, "Chance-constrained collision avoidance for mavs in dynamic environments," *IEEE Robotics and Automation Letters*, vol. 4, no. 2, pp. 776–783, 2019.
- [22] S. H. Arul, J. J. Park, and D. Manocha, "Ds-mpepc: Safe and deadlock-avoiding robot navigation in cluttered dynamic scenes," in *2023 IEEE/RSJ International Conference on Intelligent Robots and Systems (IROS)*. IEEE, 2023, pp. 2256–2263.
- [23] C. E. Luis and A. P. Schoellig, "Trajectory generation for multiagent point-to-point transitions via distributed model predictive control," *IEEE Robotics and Automation Letters*, vol. 4, no. 2, pp. 375–382, 2019.
- [24] M. Kloock and B. Alrifae, "Coordinated cooperative distributed decision-making using synchronization of local plans," *IEEE Transactions on Intelligent Vehicles*, vol. 8, no. 2, pp. 1292–1306, 2023.
- [25] Y. Chen, C. Wang, M. Guo, and Z. Li, "Multi-robot trajectory planning with feasibility guarantee and deadlock resolution: An obstacle-dense

- environment,” *IEEE Robotics and Automation Letters*, vol. 8, no. 4, pp. 2197–2204, 2023.
- [26] E. Trevisan and J. Alonso-Mora, “Biased-mpci: Informing sampling-based model predictive control by fusing ancillary controllers,” *IEEE Robotics and Automation Letters*, 2024.
- [27] Y. M. Chung, H. Youssef, and M. Roidl, “Distributed timed elastic band (dteb) planner: Trajectory sharing and collision prediction for multi-robot systems,” in *2022 International Conference on Robotics and Automation (ICRA)*. IEEE, 2022, pp. 10702–10708.
- [28] D. Zhou, Z. Wang, S. Bandyopadhyay, and M. Schwager, “Fast, on-line collision avoidance for dynamic vehicles using buffered voronoi cells,” *IEEE Robotics and Autom. Letters*, vol. 2, no. 2, pp. 1047–1054, 2017.
- [29] H. Zhu and J. Alonso-Mora, “B-uavc: Buffered uncertainty-aware voronoi cells for probabilistic multi-robot collision avoidance,” in *2019 international symposium on multi-robot and multi-agent systems (MRS)*. IEEE, 2019, pp. 162–168.
- [30] M. Abdulkhak and A. Vardy, “Deadlock prediction and recovery for distributed collision avoidance with buffered voronoi cells,” in *2021 IEEE/RSJ International Conference on Intelligent Robots and Systems (IROS)*. IEEE, 2021, pp. 429–436.
- [31] A. Pierson, W. Schwarting, S. Karaman, and D. Rus, “Weighted buffered voronoi cells for distributed semi-cooperative behavior,” in *2020 IEEE international conference on robotics and automation (ICRA)*. IEEE, 2020, pp. 5611–5617.
- [32] J.-L. Bastarache, C. Nielsen, and S. L. Smith, “On legible and predictable robot navigation in multi-agent environments,” in *2023 IEEE international conference on robotics and automation (ICRA)*. IEEE, 2023, pp. 5508–5514.
- [33] C. I. Mavrogiannis and R. A. Knepper, “Multi-agent path topology in support of socially competent navigation planning,” *The International Journal of Robotics Research*, vol. 38, no. 2-3, pp. 338–356, 2019.
- [34] B. Şenbaşlar, W. Hönig, and N. Ayanian, “Rlss: real-time, decentralized, cooperative, networkless multi-robot trajectory planning using linear spatial separations,” *Autonomous Robots*, pp. 1–26, 2023.
- [35] J. Park, I. Jang, and H. J. Kim, “Decentralized deadlock-free trajectory planning for quadrotor swarm in obstacle-rich environments—extended version,” *arXiv preprint arXiv:2209.09447*, 2022.
- [36] A. Patwardhan, R. Murai, and A. J. Davison, “Distributing collaborative multi-robot planning with gaussian belief propagation,” *IEEE Robotics and Automation Letters*, vol. 8, no. 2, pp. 552–559, 2023.
- [37] M. Čáp, J. Vokřínek, and A. Kleiner, “Complete decentralized method for on-line multi-robot trajectory planning in well-formed infrastructures,” in *Proceedings of the international conference on automated planning and scheduling*, vol. 25, 2015, pp. 324–332.
- [38] K. Kondo, J. Tordesillas, R. Figueroa, J. Rached, J. Merkel, P. C. Lusk, and J. P. How, “Robust mader: Decentralized and asynchronous multiagent trajectory planner robust to communication delay,” in *2023 IEEE International Conference on Robotics and Automation (ICRA)*. IEEE, 2023, pp. 1687–1693.
- [39] B. Şenbaşlar and G. S. Sukhatme, “Dream: Decentralized real-time asynchronous probabilistic trajectory planning for collision-free multi-robot navigation in cluttered environments,” *arXiv preprint arXiv:2307.15887*, 2023.
- [40] Y. Chen, M. Guo, and Z. Li, “Deadlock resolution and recursive feasibility in mpc-based multi-robot trajectory generation,” *IEEE Transactions on Automatic Control*, 2024.
- [41] Y. Chen, H. Dong, and Z. Li, “Asynchronous spatial allocation protocol for trajectory planning of heterogeneous multi-agent systems,” *arXiv preprint arXiv:2309.07431*, 2023.
- [42] V. K. Adajania, S. Zhou, A. K. Singh, and A. P. Schoellig, “Amswarm: An alternating minimization approach for safe motion planning of quadrotor swarms in cluttered environments,” in *International Conference on Robotics and Automation (ICRA)*. IEEE, 2023, pp. 1421–1427.
- [43] C. Toumich and D. Floreano, “High-speed motion planning for aerial swarms in unknown and cluttered environments,” *arXiv preprint arXiv:2402.19033*, 2024.
- [44] J. Orr and A. Dutta, “Multi-agent deep reinforcement learning for multi-robot applications: A survey,” *Sensors*, vol. 23, no. 7, p. 3625, 2023.
- [45] Y. F. Chen, M. Liu, M. Everett, and J. P. How, “Decentralized non-communicating multiagent collision avoidance with deep reinforcement learning,” in *2017 IEEE international conference on robotics and automation (ICRA)*. IEEE, 2017, pp. 285–292.
- [46] Y. F. Chen, M. Everett, M. Liu, and J. P. How, “Socially aware motion planning with deep reinforcement learning,” in *2017 IEEE/RSJ International Conference on Intelligent Robots and Systems (IROS)*. IEEE, 2017, pp. 1343–1350.
- [47] R. Han, S. Chen, S. Wang, Z. Zhang, R. Gao, Q. Hao, and J. Pan, “Reinforcement learned distributed multi-robot navigation with reciprocal velocity obstacle shaped rewards,” *IEEE Robotics and Automation Letters*, vol. 7, no. 3, pp. 5896–5903, 2022.
- [48] Z. Xie and P. Dames, “Drl-vo: Learning to navigate through crowded dynamic scenes using velocity obstacles,” *IEEE Transactions on Robotics*, vol. 39, no. 4, pp. 2700–2719, 2023.
- [49] R. Han, S. Chen, and Q. Hao, “Cooperative multi-robot navigation in dynamic environment with deep reinforcement learning,” in *International Conference on Robotics and Automation (ICRA)*. IEEE, 2020, pp. 448–454.
- [50] T. Fan, P. Long, W. Liu, and J. Pan, “Distributed multi-robot collision avoidance via deep reinforcement learning for navigation in complex scenarios,” *The International Journal of Robotics Research*, vol. 39, no. 7, pp. 856–892, 2020.
- [51] Q. Tan, T. Fan, J. Pan, and D. Manocha, “Deepmnavigate: Deep reinforced multi-robot navigation unifying local & global collision avoidance,” in *2020 IEEE/RSJ International Conference on Intelligent Robots and Systems (IROS)*. IEEE, 2020, pp. 6952–6959.
- [52] P. Long, T. Fan, X. Liao, W. Liu, H. Zhang, and J. Pan, “Towards optimally decentralized multi-robot collision avoidance via deep reinforcement learning,” in *2018 IEEE international conference on robotics and automation (ICRA)*. IEEE, 2018, pp. 6252–6259.
- [53] B. Brito, M. Everett, J. P. How, and J. Alonso-Mora, “Where to go next: Learning a subgoal recommendation policy for navigation in dynamic environments,” *IEEE Robotics and Automation Letters*, vol. 6, no. 3, pp. 4616–4623, 2021.
- [54] C. Chen, Y. Liu, S. Kreiss, and A. Alahi, “Crowd-robot interaction: Crowd-aware robot navigation with attention-based deep reinforcement learning,” in *2019 international conference on robotics and automation (ICRA)*. IEEE, 2019, pp. 6015–6022.
- [55] M. Everett, Y. F. Chen, and J. P. How, “Motion planning among dynamic, decision-making agents with deep reinforcement learning,” in *2018 IEEE/RSJ International Conference on Intelligent Robots and Systems (IROS)*. IEEE, 2018, pp. 3052–3059.
- [56] J. Qin, J. Qin, J. Qiu, Q. Liu, M. Li, and Q. Ma, “Srl-orca: A socially aware multi-agent mapless navigation algorithm in complex dynamic scenes,” *IEEE Rob. and Autom. Lett.*, vol. 9, no. 1, pp. 143–150, 2023.
- [57] Q. Li, F. Gama, A. Ribeiro, and A. Prorok, “Graph neural networks for decentralized multi-robot path planning,” in *2020 IEEE/RSJ International Conference on Intelligent Robots and Systems (IROS)*. IEEE, 2020, pp. 11785–11792.
- [58] L. Chen, Y. Wang, Z. Miao, M. Feng, Z. Zhou, H. Wang, and D. Wang, “Toward safe distributed multi-robot navigation coupled with variational bayesian model,” *IEEE Transactions on Automation Science and Engineering*, 2023.
- [59] J. Gielis, A. Shankar, and A. Prorok, “A critical review of communications in multi-robot systems,” *Current Robotics Reports*, vol. 3, no. 4, pp. 213–225, 2022.
- [60] M. Bolderer, L. Palopoli, and D. Fontanelli, “Lloyd-based approach for robots navigation in human-shared environments,” in *2020 IEEE/RSJ International Conference on Intelligent Robots and Systems (IROS)*. IEEE, 2020, pp. 6982–6989.
- [61] Á. Serra-Gómez, E. Montijano, W. Böhmer, and J. Alonso-Mora, “Active classification of moving targets with learned control policies,” *IEEE Robotics and Automation Letters*, vol. 8, no. 6, pp. 3717–3724, 2023.
- [62] M. Bolderer, A. Antonucci, P. Bevilacqua, L. Palopoli, and D. Fontanelli, “Multi-agent navigation in human-shared environments: A safe and socially-aware approach,” *Robotics and Autonomous Systems*, vol. 149, p. 103979, 2022.
- [63] S. Lloyd, “Least squares quantization in pcm,” *IEEE transactions on information theory*, vol. 28, no. 2, pp. 129–137, 1982.
- [64] J. Cortes, S. Martinez, T. Karatas, and F. Bullo, “Coverage control for mobile sensing networks,” *IEEE Transactions on robotics and Automation*, vol. 20, no. 2, pp. 243–255, 2004.
- [65] M. Bolderer, D. Fontanelli, and L. Palopoli, “Coverage control and distributed consensus-based estimation for mobile sensing networks in complex environments,” in *2019 IEEE 58th Conference on Decision and Control (CDC)*. IEEE, 2019, pp. 7838–7843.
- [66] M. Bolderer, P. Bevilacqua, L. Palopoli, and D. Fontanelli, “Graph connectivity control of a mobile robot network with mixed dynamic multi-tasks,” *IEEE Rob. and Autom. Lett.*, vol. 6, no. 2, pp. 1934–1941, 2021.
- [67] M. Bolderer, L. Palopoli, and D. Fontanelli, “A unified lloyd-based framework for multi-agent collective behaviours,” *Robotics and Autonomous Systems*, vol. 156, p. 104207, 2022.

- [68] J. Lee, Y. Lee, J. Kim, A. Kosiorek, S. Choi, and Y. W. Teh, "Set transformer: A framework for attention-based permutation-invariant neural networks," in *Int. Conf. on Mach. Learn.*, 2019, pp. 3744–3753.
- [69] J. Schulman, F. Wolski, P. Dhariwal, A. Radford, and O. Klimov, "Proximal policy optimization algorithms," *ArXiv*, vol. abs/1707.06347, 2017.
- [70] E. Liang *et al.*, "RLlib: Abstractions for distributed reinforcement learning," in *Int. Conf. on Mach. Lear.*, 2018.
- [71] T. Haarnoja, H. Tang, P. Abbeel, and S. Levine, "Reinforcement learning with deep energy-based policies," in *Proceedings of the 34th International Conference on Machine Learning (ICML)*, 2017.
- [72] R. S. Sutton and A. G. Barto, *Reinforcement learning: An introduction*. MIT press, 2018.
- [73] H. Zhu, B. Brito, and J. Alonso-Mora, "Decentralized probabilistic multi-robot collision avoidance using buffered uncertainty-aware voronoi cells," *Autonomous Robots*, vol. 46, no. 2, pp. 401–420, 2022.
- [74] J. van den Berg, S. J. Guy, J. Snape, M. C. Lin, and D. Manocha, "Rvo2 library: Reciprocal collision avoidance for real-time multi-agent simulation," See <https://gamma.cs.unc.edu/RVO2>, 2011.
- [75] S. Zhang, O. So, K. Garg, and C. Fan, "Gcbf+: A neural graph control barrier function framework for distributed safe multi-agent control," *arXiv preprint arXiv:2401.14554*, 2024.
- [76] C. E. Luis, M. Vukosavljev, and A. P. Schoellig, "Online trajectory generation with distributed model predictive control for multi-robot motion planning," *IEEE Robotics and Automation Letters*, vol. 5, no. 2, pp. 604–611, 2020.
- [77] J. Park, D. Kim, G. C. Kim, D. Oh, and H. J. Kim, "Online distributed trajectory planning for quadrotor swarm with feasibility guarantee using linear safe corridor," *IEEE Robotics and Automation Letters*, vol. 7, no. 2, pp. 4869–4876, 2022.
- [78] V. Walter, N. Staub, A. Franchi, and M. Saska, "Uvdar system for visual relative localization with application to leader-follower formations of multirotor uavs," *IEEE Robotics and Automation Letters*, vol. 4, no. 3, pp. 2637–2644, 2019.
- [79] D. Hert *et al.*, "Mrs modular uav hardware platforms for supporting research in real-world outdoor and indoor environments," in *2022 International Conference on Unmanned Aircraft Systems (ICUAS)*. IEEE, 2022, pp. 1264–1273.
- [80] —, "Mrs drone: A modular platform for real-world deployment of aerial multi-robot systems," *Journal of Intelligent & Robotic Systems*, vol. 108, no. 4, p. 64, 2023.
- [81] T. Baca *et al.*, "The mrs uav system: Pushing the frontiers of reproducible research, real-world deployment, and education with autonomous unmanned aerial vehicles," *Journal of Intelligent & Robotic Systems*, vol. 102, no. 1, p. 26, 2021.

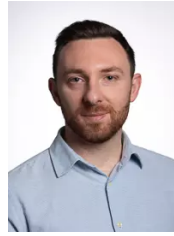


interests include mobile robotics, distributed control and multi-agent systems.

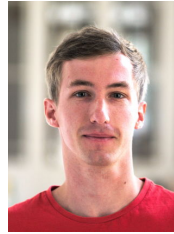
Manuel Boldrer received the Ph.D degree in Mechatronics and Systems Engineering from the University of Trento, Trento, Italy, in 2022. He was a Visiting Scholar at the University of California, Riverside, Riverside, US, in 2021. He was a Postdoctoral Researcher with the Cognitive Robotics Department (CoR), Delft University of Technology, Delft, The Netherlands, in the Reliable Robot Control Lab from 2022 to 2023. As of today, he is a Researcher at the Multi Robot System group (MRS), Czech Technical University, Prague, Czechia. His research



Álvaro Serra-Gómez is a Ph.D. student at the Department of Cognitive Robotics at the Delft University of Technology. He received his M.Sc. (2019) both at the Polytechnic University of Catalonia in Automatic Control and Robotics and at the École Polytechnique de Paris in Data Science in the Computer Science and Applied Mathematics Departments. His current research focuses on learning hierarchical motion planning policies to coordinate multi-robot systems in active perception and collision avoidance tasks.



Lorenzo Lyons received the M.Sc. degree in mechanical engineering from the Polytechnic University of Milan, Milan, Italy, in 2021. He is currently pursuing the Ph.D. degree with the Cognitive Robotics (CoR) Department, Delft University of Technology, Delft, The Netherlands. His research interests include numerical optimization, model predictive control, multi-robot motion planning applied to the automotive, and robotics.



Vít Krátký received the M.Sc. degree in Cybernetics and Robotics in 2019, and the Ph.D. degree in Informatics in 2024, both from the Czech Technical University in Prague, Czech Republic. Currently he works as a researcher with the Multi-Robot Systems Group at CTU in Prague. His research interests include cooperative motion planning, multi-agent systems, and autonomous navigation of unmanned aerial vehicles.



Javier Alonso-Mora received the Ph.D. degree in robotics on cooperative motion planning from ETH Zurich, Zurich, Switzerland, in partnership with Disney Research Studios, Zurich, Switzerland. He is currently an Associate Professor with the Delft University of Technology, Delft, The Netherlands, where he leads the Autonomous Multi-robots Lab. He was a Postdoctoral Associate at the Computer Science and Artificial Intelligence Lab (CSAIL), Massachusetts Institute of Technology, Cambridge, MA, USA. His research interests include navigation, motion planning, and control of autonomous mobile robots, with a special emphasis on multirobot systems, mobile manipulation, on-demand transportation, and robots that interact with other robots and humans in dynamic and uncertain environments. Dr. Alonso-Mora is an Associate Editor for IEEE TRANSACTIONS ON ROBOTICS and for Springer Autonomous Robots. He was the recipient of a talent scheme VENI Award from the Netherlands Organization for Scientific Research (2017), ICRA Best Paper Award on Multi-robot Systems (2019), and an ERC Starting Grant (2021)



Laura Ferranti received the Ph.D. degree in control engineering from the Delft University of Technology, Delft, The Netherlands, in 2017. She is currently an Assistant Professor with the Cognitive Robotics (CoR) Department, Delft University of Technology. Her research interests include optimization and optimal control, model predictive control, reinforcement learning, embedded optimization-based control with application in flight control, maritime transportation, robotics, and automotive. Dr. Ferranti was a recipient of the NWO Veni Grant from the Netherlands Organization for Scientific Research in 2020 and the Best Paper Award on Multi-Robot Systems at International Conference on Robotics and Automation (ICRA) 2019